TR-11
1968

Studies of Turbulence in Shallow Sediment Laden Flow with Superimposed Rainfall

B.J. Barfield

Texas Water Resources Institute

Texas A&M University

STUDIES OF TURBULENCE IN SHALLOW SEDIMENT LADEN FLOW WITH SUPERIMPOSED RAINFALL

By

BILLY JOE BARFIELD

Technical Report No. 11
Water Resources Institute
Texas A&M University
January 1968

The investigations leading to this report were a portion of the research under Research Grant Number WP-00757-03, Federal Water Pollution Control Administration, U. S. Department of the Interior, with Dr. Ernest T. Smerdon as principal investigator. The research was performed in the Agricultural Engineering Research Laboratory, Texas A&M University, College Station, Texas.

FOREWORD

This investigation was a part of a research project to study the mechanism of sediment transport in that zone where runoff flow is shallow and flow conditions may be significantly changed by the energy of rainfall impinging on the free surface of the flow. The title of the research project was "Water Pollution from Eroded Sediments." In this project, the transport of eroded sediments from the point of initial detachment from the soil to a stream of sufficient size that rainfall would not significantly affect flow conditions was studied.

Since suspended sediment transport is dependent on turbulence to keep the sediment in suspension, investigations of turbulence became a major part of the project. The project resulted in the development of a sediment transport model derived from turbulent diffusion theory. Although the tests did not confirm the model as being adequate, several problems arose which require further study before the model should be rejected. We are encouraged about the possibility of explaining sediment transport by a stochastic model derived from turbulent diffusion theory. We hope that studies beyond the scope possible in the research reported herein can be conducted on this important sediment transport problem.

ABSTRACT

Studies of Turbulence in Shallow Sediment Laden Flow with Superimposed Rainfall. (May 1968)

Billy J. Barfield, B. S., Texas A&M University

Directed by: Dr. Ernest T. Smerdon

The structure of turbulence has been shown to affect the sediment carrying capability of streams. Due to the random nature of turbulence, sediment movement was analyzed as a stochastic process. Starting with the Langevin equation modified for a turbulent medium, a partial differential equation was developed as a mathematical model which describes the change in sediment concentration with time and space for two dimensional open channel flow with isotropic turbulence. The input parameters to the partial differential equation were the particle fall velocity and the turbulent diffusion coefficient. The diffusion coefficient used was the product of the mean square velocity and the Eulerian time scale of turbulence.

A 40 ft. recirculating research flume was used for the experimental investigations. The RMS velocity and Eulerian time scale profiles were determined by use of a hot-film anemometer and a random signal correlator. The effect of rainfall on the RMS velocities and time scale profiles was observed. Sediment concentration profiles were measured by withdrawing samples from the flow and were compared with values predicted by the derived mathematical model.

ACKNOWLEDGEMENTS

Grateful acknowledgement is first of all expressed to my wife, Annette, for her continual patience, encouragement, and assistance.

Gratitude is expressed to Dr. E. T. Smerdon who originally encouraged the research and provided continual guidance throughout the investigations.

Dr. E. A. Hiler is thanked for his instruction in the area of turbulent diffusion and for his counsel on experimental procedures.

The review of the dissertation and the helpful suggestions by Drs. Bloodworth, Bryant, Clark, and Davis are appreciated.

Gratitude is further expressed to the Federal Water Pollution Control Administration for their support of the project and for their assistantship.

TABLE OF CONTENTS

Chapter		Page
I	INTRODUCTION	1
II	LITERATURE REVIEW	4
	Semi-Empirical Theories of Sediment Transportation	4
	Statistical Theories of Turbulent Diffusion	4
	Particle Displacement in Turbulent Shear Flow	5
	The Effects of Rainfall on Sediment Transportation	5
III	THEORETICAL DEVELOPMENT	7
	Equation of Motion of a Discrete Particle	7
	The Development of the Diffusion Equation for the Field Free Case	11
	Batchelor's Method	11
	Use of the Justified Langevin Equation	13
	Development of a Partial Differential Equation for the Case of a Gravity Force Field	18
	Adaptation of the Equation to Two Dimensional Flow	23
IV	EXPERIMENTAL PROCEDURES	25
	Description of the Flume and Materials	25
	Research Flume	25
	Materials	29
	Turbulence Measurements	31
	Hot-Film Anemometer	31
	Calibration	36

Chapter		Page
	Measurements of Time Scale of Turbulence	40
	Measurement of RMS Velocities	43
	Sediment Concentration Measurements	45
	Method of Collecting Samples	45
	Method of Measuring Concentrations	45
V	RESULTS AND DISCUSSION	47
	Turbulence Characteristics of the Flow	47
	Time Scale of Turbulence	47
	RMS Velocity Profiles	57
	Diffusion Coefficient as a Function of Depth	63
	The Effects of Superimposed Rainfall on the Structure of Turbulence	70
	Prediction of Sediment Profiles from Turbulence Data	71
	Comparison of Predicted Versus Observed Concentrations	73
	Possible Sources of Error in Input Turbulence Parameters	73
	Possible Errors in the Mathematical Model	81
VI	SUMMARY AND CONCLUSIONS	83
	APPENDIX A SOME THEORETICAL RELATIONSHIPS USED IN FORMULATING THE MATHEMATICAL MODEL	86
	APPENDIX B SUMMARY OF DATA	91
	GLOSSARY OF SYMBOLS	100
	LITERATURE CITED	104

LIST OF TABLES

Table		Page
1	Hydraulic Parameters for the Tests	26
2	Physical Properties of Glass Beads	32
3	Equations Used for the Computer Solution	74
4	Summary of Data Test 1A High	92
5	Summary of Data Test 1B High	93
6	Summary of Data Test 1A Low	94
7	Summary of Data Test 1B Low	95
8	Summary of Data Test 2A High	96
9	Summary of Data Test 2B High	97
10	Summary of Data Test 2A Low	98
11	Summary of Data Test 2B Low	99

LIST OF FIGURES

Figure		Page
1	Force Per Unit Mass on a Fluid Particle in a Turbulent Medium	9
2	Schematic of Research Flume	27
3	Overall View of Research Flume	28
4	Isolines of Rainfall on the Water Surface	30
5	Microphotograph of Glass Beads	33
6	Constant Temperature Anemometer	34
7	Pressure Transducer and Transducer Indicator	35
8	Photograph of Hot-Film Sensor and Pitot Tube in the Flume	37
9	Schematic of Calibration Arrangement	38
10	Bridge DC Drift for TSI Cylindrical Sensor	38
11	Calibration Curves for TSI Cylindrical Sensor	41
12	Schematic of Velocity and Turbulence Instrumentation.	42
13	Typical Correlogram as Photographed on the Oscilloscope Display	44
14	Prandtl Tube and Point Sediment Sampler	46
15	Eulerian Time Scale Profiles for Tests 1A High and 1B High	48
16	Eulerian Time Scale Profiles for Tests 1A Low and 1B Low	49
17	Eulerian Time Scale Profiles for Tests 2A High and 2B High	50
18	Eulerian Time Scale Profiles for Tests 2A Low and 2B Low	51

Figure		Page
19	Correlograms for Tests 1A High and 1B High.....	53
20	Correlograms for Tests 1A Low and 1B Low.....	54
21	Correlograms for Tests 2A High and 2B High.....	55
22	Correlograms for Tests 2A Low and 2B Low.....	56
23	Turbulent Intensity Profiles for Tests 1A High and 1B High.....	59
24	Turbulent Intensity Profile for Tests 1A Low and 1B Low and Comparison with Raichlen's Data.....	60
25	Turbulent Intensity Profiles for Tests 2A High and 2B High.....	61
26	Turbulent Intensity Profiles for Tests 2A Low and 2B Low.....	62
27	Comparison Between Turbulent Intensities for Test 1A High and Data Obtained by Rao.....	64
28	Diffusion Coefficient Profiles for Tests 1A High and 1B High.....	66
29	Diffusion Coefficient Profiles for Tests 1A Low and 1B Low.....	67
30	Diffusion Coefficient Profiles for Tests 2A High and 2B High.....	68
31	Diffusion Coefficient Profiles for Tests 2A Low and 2B Low.....	69
32	Predicted Concentrations for Test 1A High.....	75
33	Predicted Concentrations for Test 1A Low.....	76
34	Predicted Concentrations for Test 2A High.....	77
35	Predicted Concentrations for Test 2A Low.....	78
36	Photograph of Flume Bed Showing Dune Formations.....	80

CHAPTER I

INTRODUCTION

The history of mankind is interwoven with the search for suitable water supplies. From the early Egyptian empire along the Nile to the modern legal battles over water in the western United States and even to the war over land near the Jordan river, the availability of usable water has exerted a strong influence on the activities of mankind.

In man's quest for usable supplies of water, reservoirs have been built to store surplus runoff. One of the major problems encountered in reservoir storage of water is the loss of storage space due to siltation by eroded sediment. Of the 33.6 million acre-feet of initial storage available in reservoirs of the Upper Colorado River Basin, 17.8 million acre-feet have been included for sediment storage pools (6). Through control of sedimentation, this costly addition could be reduced.

One of the problems encountered in the removal of sediment from water is the inability to predict sediment profiles as a function of flow conditions. This difficulty generally limits sediment removal studies to trial and error procedures.

The movement of sediment from the initial point of detachment to its place of final deposition is effected through several processes. After its initial detachment, a sediment particle moves along in a shallow channel either as suspended load or as bed load. Bed load

can be defined as that material which is moved by rolling or sliding at the stream bed. Suspended material is that material which is intermittently or continously detached from the bed, placed in suspension by the fluid turbulence, and redeposited in the channel.

After a particle is eroded and begins to be transported the flow is quite often subjected to intense superimposed rainfall containing a large amount of energy which must be dissipated. This energy dissipation can alter the sediment carrying capacity of the flow.

As these shallow channels merge to form deeper channels, the sediment is still carried as suspended material or bed load. It is conceivable that superimposed rainfall would have little effect on the sediment carrying capability in the deeper flows. The sediment is further carried along in the stream until it reaches the reservoir or large body of water where the absence of turbulence allows it to be finally deposited.

Most of the past research on detachment and movement of sediment has been oriented toward a look at average conditions and gross mechanics. The research reported herein had as its purpose a stochastic description of the movement of particles in a turbulent medium. Through this theoretical description, the movement of an ensemble of particles is investigated and finally an equation is formulated to describe the concentration of sediment as a function

of time and space in a turbulent medium. Experimental investigations of the validity of the mathematical model were conducted in a 40 ft. research flume with rainfall simulation capability.

The research had as a further objective the study of the effect of superimposed rainfall on the sediment diffusive capability of shallow open channel flow.

C H A P T E R I I

LITERATURE REVIEW

Sediment transportation as viewed from turbulent diffusion theory involves two areas in which a large amount of literature exists, vis., turbulence and transport processes. Consequently, only research which directly applies to this report will be discussed.

Semi-Empirical Theories of Sediment Transportation

O'Brien postulated a steady state differential equation for sediment transport in 1933 and Rouse solved the equation in 1937, assuming a logarithmic velocity profile and an equality between the sediment and momentum diffusion coefficients (14, 17). Vanoni investigated the validity of Rouse's solution in 1946 and found that the sediment diffusion coefficient and the momentum diffusion coefficient were of the same form, but slightly different in magnitudes (21). Leliavsky has summarized and discussed the more important suspended load and bed load formulas (11).

Statistical Theories of Turbulent Diffusion

Taylor in 1920 first described the root-mean square particle displacement for uni-directional dispersion by turbulent motion (19). Kampé de Fériet in 1939 performed a partial integration of Taylor's equation which yielded the result that the root-mean-square displacement is proportional to the square of time for very small times and proportional to time for very large times (10).

Batchelor extended the analysis to three dimensions in 1949 and derived an expression for the concentration as a function of time for a fluid property unaffected by external force fields (1). In his analysis, Batchelor assumes a normal distribution of displacement of fluid particles. Since the approach of Batchelor is similar to that used in this research, his theory will be discussed in more detail in the next chapter.

Particle Displacement in Turbulent Shear Flow

The displacement of a fluid particle in turbulent flow from some initial position is discussed by Batchelor in several papers on diffusion (1, 2). Based on a heuristic appeal to the Central Limit Theorem, he shows that the probability density function for the displacement should be Gaussian for a fluid particle whose velocity is covariant stationary. Townsend reports on numerous measurements of the probability density function for displacement in isotropic turbulence showing them to be Gaussian (20).

The Effects of Rainfall on Sediment Transportation

Smerdon observed the values of critical tractive force -- the force required to initiate erosion -- in 1963 with rainfall superimposed on the water surface (19). He concluded that rainfall slightly increased the critical tractive force as calculated from the depth of flow and channel slope. This would indicate that rainfall decreased the tendency for flow to erode the bed.

Glass investigated the effects of rainfall on the logarithmic velocity profile in 1965 and found that the velocity at the surface was retarded, the velocity gradient reduced, and the bed shear reduced by rainfall (7). His tests also indicated that rainfall increased von Karman's constant.

No known information is available concerning the effect of rainfall on the motion of individual particles. Therefore, the work which is reported herein had a three-fold objective; to develop a theoretical relationship for the diffusion of sediment particles, to test the validity of the model, and to see how this diffusion would be affected by rainfall.

CHAPTER III

THEORETICAL DEVELOPMENT

The theoretical development of the equation for turbulent diffusion of discrete particles is divided into three sections. First, a differential equation for the motion of an individual fluid particle is considered in terms of the forces imparted by the turbulent medium. This equation, usually referred to as the Langevin equation, is integrated for the theoretical case of zero gravity to find the expected values of the mean square displacements of a particle with time. The second section concerns the development of a partial differential equation for the turbulent diffusion of particles using two alternate approaches. The first approach developed by Batchelor uses a Gaussian distribution for particle displacement (1). The second approach uses a mean square displacement obtained from the integrated Langevin equation. Comparison of the two methods allows inference of the constants of integration for the Langevin equation. These constants are used in the final section for the development of a partial differential equation for turbulent diffusion with a gravitational force field.

Equation of Motion of a Discrete Particle

If one assumes that the forces imparted on a discrete fluid particle by a turbulent medium can be separated into two statistically independent components, then a stochastic differential equation[1] can be

[1] A stochastic differential equation is one whose forcing function is described probabilistically rather than deterministically.

derived for the motion of a particle. Figure 1 shows the forces acting on a particle. These forces are related by Newton's second law as

$$\frac{d\underline{v}(t)}{dt} = \underline{A}(t) - \beta\, \underline{v}(t) - \left(1 - \frac{\rho_o}{\rho}\right) \underline{g} \qquad (1)$$

in which $\underline{v}(t)$ is the instantaneous particle velocity, $\underline{A}(t)$ is some rapidly fluctuating term which represents the accelerative forces imparted to the particle by the fluid turbulence, β is a drag coefficient, ρ_o the fluid density, ρ is the particle density, and g is the acceleration due to gravity. This equation is similar to the Langevin equation for Brownian motion with an external force field.

The drag coefficient is assumed to be a constant over the range of velocities considered. Since the velocities concerned are the turbulent fluctuations, it will be assumed that the range of velocities are such that can be represented by Stokes' coefficient of $\frac{18\mu}{\rho_o d^2}$ in which is the dynamic viscosity, ρ_o the fluid density, and d the diameter of the particle.

In this section, only the field free case when gravity is neglected will be considered in order to show the validity of the representation given by equation (1). In the absence of gravity equation (1) becomes

$$\frac{d\underline{v}(t)}{dt} = \underline{A}(t) - \beta\underline{v}(t) \quad . \qquad (1a)$$

Equation (1a) has the solution

$$\underline{v}(t) = \underline{v}_o e^{-\beta t} + e^{-\beta t} \int_0^t e^{\beta\tau}\, \underline{A}(\varepsilon)\, d\varepsilon \qquad (2)$$

in which $\underline{v}_o$ is the initial particle velocity, and the other terms are as previously defined. Integrating the velocity to obtain the

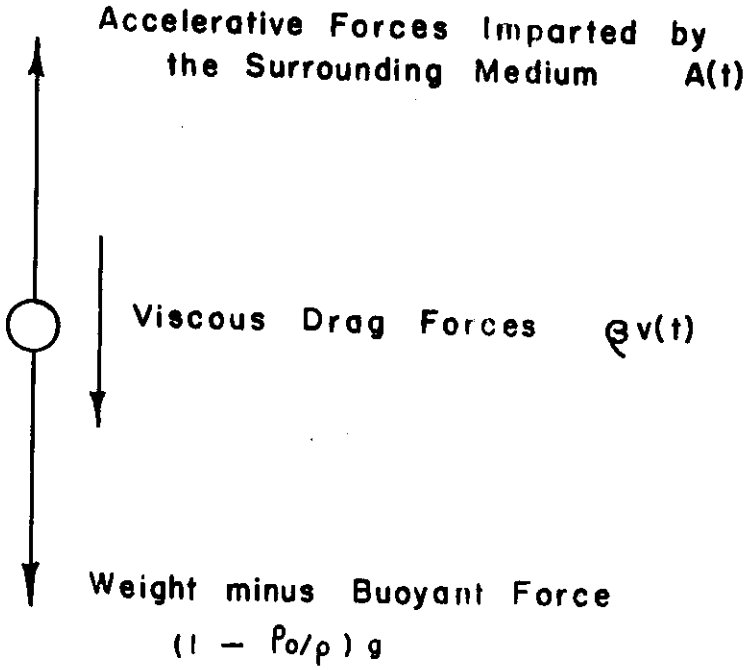

Figure 1. Force Per Unit Mass on a Fluid Particle in a Turbulent Medium

displacement, $\underline{X}(t)$, yields

$$\underline{X}(t) = \frac{\underline{v}_o}{\beta}\left[1 - e^{-\beta t}\right] + \int_o^t e^{-\beta\tau} \int_o^t e^{-\beta\varepsilon}\underline{A}(\varepsilon)d\varepsilon d\tau \quad . \quad (3)$$

Integrating by parts simplifies equation (3) to

$$\underline{X}(t) = \frac{\underline{v}_o}{\beta}\left[1 - e^{-\beta t}\right] + \frac{1}{\beta}\int_o^t \underline{A}(\tau)d\tau - \frac{1}{\beta}\, e^{-\beta t}\int_o^t e^{-\beta\tau}\underline{A}(\tau)d\tau \quad . \quad (4)$$

Taking the expected value of $\underline{X}(t)$ yields

$$\overline{\underline{X}(t)} = \frac{\underline{v}_o}{\beta}\left[1 - e^{-\beta t}\right] \quad (5)$$

in which the overbar denotes statistical expectation.

With statistical descriptions, the second moments are of prime interest. With this representation for the equation of motion of a particle, it is also of interest to determine if the second moment is that described by Taylor in 1920. The second moment of $\underline{X}(t)$ is

$$\underline{X}^2(t) = \frac{\underline{v}_o^2}{\beta^2}\left[1 - e^{-\beta t}\right] + \frac{1}{\beta^2}\, e^{-\beta t}\int_o^t\int_o^t e^{\beta(t+\varepsilon)}\,\overline{\underline{A}(\tau)\underline{A}(\varepsilon)}d\tau d\varepsilon$$
$$+ \frac{1}{\beta^2}\int_o^t\int_o^t \overline{\underline{A}(\tau)\underline{A}(\varepsilon)}d\tau d\varepsilon - \frac{2}{\beta^2}\, e^{-\beta t}\int_o^t\int_o^t e^{\beta\tau}\,\overline{\underline{A}(\tau)\underline{A}(\varepsilon)}d\tau d\varepsilon$$
$$+ \frac{2\underline{v}_o}{\beta}\left[1 - e^{-\beta t}\right]\left[\frac{1}{\beta}\int_o^t \underline{A}(\tau)d\tau - \frac{1}{\beta^2}\, e^{-\beta t}\int_o^t e^{\beta\tau}\,\underline{A}(\tau)d\tau\right] \quad . \quad (6)$$

The expectation of $\underline{X}^2(t)$ becomes simplified somewhat if one assumes that $\underline{A}(t)$ has the following properties:

a. $\underline{A}(t)$ is a covariant stationary process

b. $\overline{\underline{v}(t)\,\underline{A}(t)} = 0$

c. $\int_o^\infty \overline{\underline{A}(\tau)\,\underline{A}(\varepsilon)}d\tau = \int_o^\infty \underline{m}(v)dv = \underline{D}$

in which $\underline{D}$ is some constant for a given turbulent medium and $\underline{m}(v)$ is the covariance kernel for $\underline{A}(t)$. These are the same properties which Chadam described in 1962 (3). By using the three properties of $\underline{A}(t)$ and by using statistical techniques characteristic of Brownian motion, Chadam showed that equation (6) reduced to

$$\overline{\underline{X}^2(t)} = \frac{\underline{v}_o^2}{\beta^2}\left[1 - e^{-\beta t}\right] + \frac{2\underline{D}t}{\beta^2} - \frac{\underline{D}}{2\beta^3}\left[4e^{-\beta t} - e^{-2\beta t} - 3\right] \tag{7}$$

Assuming that $\underline{v}_o = 0$, equation (7) becomes

$$\overline{\underline{X}^2(t)} = \frac{2\underline{D}t}{\beta^2} + \frac{\underline{D}}{2\beta^3}\left[4e^{-\beta t} - e^{-2\beta t} - 3\right] . \tag{8}$$

For large t, equation (8) becomes

$$\overline{\underline{X}^2(t)} = \frac{2\underline{D}t}{\beta^2} \tag{9}$$

which is of the same form that Taylor obtained in 1920 considering only turbulent fluid velocities. Therefore, it seems reasonable that $\underline{A}(t)$ possesses the properties listed, and the representation given by equation (1) for the motion of a discrete particle is justified.

The Development of the Diffusion Equation for the Field Free Case

The development of a partial differential equation for diffusion in the gravity free case is presented in this section since it yields relationships essential to the development of an equation for the case of a gravity force field.

Batchelor's Method. If the properties of conditional probability are used, the probability that a particle will be located at $\underline{x}$ at time t can be written as

$$P[\underline{x}(t)] = \int P[\underline{x}(t_o)]\ Q\ [\underline{x}(t) - \underline{x}(t_o) \mid \underline{x}(t_o)]\ d\underline{x}_o \qquad (10)$$

in which $P[\underline{x}(t_o)]$ is the probability of a particle being located at $\underline{x}$ at time t_o and Q is the conditional probability distribution function for displacement $\underline{x}(t) - \underline{x}(t_o)$ when given $\underline{x}(t_o)$. It should be noted that x refers to space whereas X refers to displacement. Equation (10) can be written alternately as the convolution

$$P[\underline{x}(t)] = P[\underline{x}(t_o)]\ *Q[x(t) \mid x(t_o)] \quad . \qquad (11)$$

Application of the Fourier transform to find the characteristic function for $P[\underline{x}(t)]$ yields

$$\Phi_{\underline{x}}(\underline{\xi}) = \Phi_{\underline{x}_o}(\underline{\xi})\ \Phi_{(\underline{x} - \underline{x}_o)}(\underline{\xi}) \qquad (12)$$

in which $\Phi_{\underline{x}}(\underline{\xi})$, $\Phi_{\underline{x}_o}(\underline{\xi})$ and $\Phi_{(\underline{x} - \underline{x}_o)}(\underline{\xi})$ are respectively the characteristic functions for $\underline{x}(t)$, $\underline{x}(t_o)$, and displacement $\underline{x}(t) - \underline{x}(t_o)$ in the time $t - t_o$. If the heuristic argument and experimental evidence quoted in Chapter II are accepted as evidence that the probability distribution of $\underline{x}(t) - \underline{x}(t_o)$ is multivariate normal, then the characteristic function for particle displacement becomes

$$\Phi_{(\underline{x} - \underline{x}_o)}(\underline{\xi}) = \exp\left[\frac{-\xi_i \xi_j}{2}\ \overline{X_i X_j}\right] \qquad (13)$$

in which the summation convention is used for repeated subscripts. Equation (13) can be substituted into equation (11) and the inverse transform taken to yield

$$P[\underline{x}(t)] = \frac{1}{8\pi^3}\iiint P[\underline{x}(t_o)]\ \exp\left[-\frac{\xi_i \xi_j}{2}\ \overline{X_i X_j}\right]\ e^{-i\ \underline{\xi}\ \underline{x}}\ d\underline{\xi} \quad . \qquad (14)$$

Since $-\xi_i \xi_j \, P[\underline{x}(t)] = \frac{\partial^2 P[\underline{x}(t)]}{\partial x_i \, \partial x_j}$ (See Appendix A1), differentiation of equation (14) with respect to time yields

$$\frac{\partial P[\,\underline{x}(t)]}{\partial t} = \left[\frac{\partial}{\partial t}[\,\overline{X_i X_j}]\right] \left[\frac{\partial^2 P[\,\underline{x}(t)]}{\partial x_i \, \partial x_j}\right] \quad . \tag{15}$$

The diffusion coefficient is $\frac{\partial}{\partial t}\,[\,\overline{X_i X_j}]$, and can be shown to be (See Appendix A 11)

$$\mu_{ij}(t) = \frac{\partial}{\partial t}\,[\overline{X_i X_j}] = \frac{1}{2}\, v_i' v_j' \int_0^t [R_{ij}(\varepsilon) + R_{ji}(\varepsilon)]\, d\varepsilon, \tag{16}$$

in which

$$R_{ij}(\varepsilon) = \frac{v_i(t) v_j(t+\varepsilon)}{v_i' \, v_j'} \tag{16a}$$

and v_i' = the root-mean-square velocity of the discrete particle.

For large t, $R_{ij}(\varepsilon) \to 0$, and $\mu_{ij} \to v_i' v_j' \, L_T$ (17)

in which L_T is the Eulerian time scale of turbulence defined as

$$L_T = \frac{1}{2} \int_0^\infty [R_{ij}(\varepsilon) + R_{ji}(\varepsilon)]\, d\varepsilon \quad . \tag{17a}$$

The final form of Batchelor's equation for large t is

$$\frac{\partial P\,[\underline{x}(t)]}{\partial t} = (v_i' v_j' L_T) \, \frac{\partial^2 P[\,\underline{x}(t)]}{\partial x_i \, \partial x_j} \quad . \tag{18}$$

Use of the Justified Langevin Equation. The procedure used here follows the one used by Batchelor up to equation (13). At this point the value for $\overline{\underline{X}^2(t)}$, as derived from the Langevin

equation and shown by equation (9), is inserted for $\overline{X_i X_j}$ yielding

$$\Phi_{(\underline{x} - \underline{x}_o)} (\underline{\xi}) = \exp \left[- \frac{\xi_i \xi_j}{2} \frac{2\underline{D}t}{\beta^2} \right] \quad . \tag{19}$$

If the inverse transform is taken as before, differentiation with respect to time will yield

$$\frac{\partial P [\underline{x}(t)]}{\partial t} = \frac{\partial}{\partial t} \left[\frac{\underline{D}t}{\beta^2} \right] \left[- \xi_i \xi_j P [\underline{x}(t)] \right] \tag{19a}$$

or

$$\frac{\partial P [\underline{x}(t)]}{\partial t} = \frac{\underline{D}}{\beta^2} \frac{\partial^2 P [\underline{x}(t)]}{\partial x_i \partial x_j} \quad . \tag{20}$$

It follows, therefore, in the absence of a gravity force field that for large t,

$$v_i' v_j' L_T = \frac{\underline{D}}{\beta^2} \quad . \tag{21}$$

It should be noted here that v_i' is the root-mean-square (RMS) velocity of the discrete particle and not the turbulent medium. Since the velocities of the fluid medium are much easier to measure than those of the particle, it is desirable to relate the two. By expressing the velocities of a discrete particle and the fluid particle in a Fourier-Stieltjes integral, Csanady (5) showed that the spectrum of the particle velocities for the field free case and that of the fluid velocities of the surrounding medium were related by

$$\Phi_p(\omega) = \frac{\beta^2}{\beta^2 + \omega^2} \Phi_f(\omega) \tag{22}$$

in which $\Phi_p(\omega)$ and $\Phi_f(\omega)$ are the spectral density functions for the fluid particle and surrounding fluid respectively and ω is the circular frequency in cycles per sec. (See Appendix A 111 for a derivation of equation (22).)

Thus for $\beta^2 >> \omega^2$ the particle spectral density may be taken to be that of the fluid with reasonable accuracy. Another way of stating equation (22) is that the particle spectral density may be assumed to be that of the surrounding fluid if the frequencies which contribute to particle energy are much less than β, the drag coefficient. Since the covariance kernel is the Fourier transform of the spectral density function, the assumption of equal spectral densities means that the covariance kernels are equal. Therefore, for the proper size particle,

$$\frac{D}{\beta^2} = u_i' u_j' L_T \tag{23}$$

where u_i' is the RMS velocity of the surrounding fluid.

Equation (23) has importance beyond ease of measurement. D in this case is a property of the surrounding fluid for a given particle size. The properties of the surrounding fluid are not expected to change when a gravitational force field is imposed on the discrete particles. It seems reasonable, therefore, from a heuristic analysis to assume that equation (23) is valid for the case of a gravitational force field also.

Before considering the case of a gravitational force field, it is necessary to consider the probability distribution of a variable which is a function of the accelerative terms $\underline{A}(t)$ in the justified Langevin equation (1a).

Equation (4) which is a solution of equation (1a) can be written as

$$\underline{X}(t) - \frac{\underline{v}_o}{\beta}\left[1 - e^{-\beta t}\right] = \frac{1}{\beta}\int_0^t \left[1 - e^{-\beta(t-\tau)}\right]\underline{A}(\tau)d\tau \quad . \tag{24}$$

Due to experimental evidence and the appeal of Batchelor to the Central Limit Theorem, $\underline{X}(t)$ for large t must be normally distributed with a variance of $\frac{2\underline{D}t}{\beta^2}$. Also, for large t, the distribution of $\underline{X}(t) - \frac{\underline{v}_o}{\beta}\left[1 - e^{-\beta t}\right]$ approaches that of $\underline{X}(t)$. Therefore, equation (24) can be written as the approximation

$$\underline{X}(t) = \lim_{\Delta\tau\to o} \frac{1}{\beta} \sum_j \left[1 - e^{-\beta(t-j\Delta\tau)}\right] \int_{j\Delta\tau}^{(j+1)\Delta\tau} \underline{A}(\varepsilon)d\varepsilon \tag{25}$$

or

$$\underline{X}(t) = \lim_{\Delta\tau\to o} \frac{1}{\beta^2} \Sigma \left[1 - e^{-\beta(t-j\Delta\tau)}\right] \underline{B}(\Delta\tau) \tag{26}$$

in which $\underline{B}(\Delta\tau) = \int_j^{(j+1)\Delta\tau} A(\varepsilon)d\varepsilon$. For $\underline{X}(t)$ to approach a Gaussian distribution for large t, it is necessary that $\underline{B}(\Delta\tau)$ have the distribution

$$f[\underline{B}(\Delta\tau)] = \frac{1}{(4\Pi\ D\Delta\tau)^{1/2}} \exp\left[-\frac{1}{4}|\ \underline{B}(\Delta\tau)\ |\ 2/\underline{D}\Delta\tau\right] \quad . \tag{27}$$

The following operations show that the use of equation (27) yields a Gaussian distribution for X(t). This is not proof of the validity of equation (27) but does lend credence for its further use.

Let

$$\underline{R} = \int_o^t \Psi(\varepsilon)\underline{A}(\varepsilon)d\varepsilon \tag{28}$$

and by a formulation similar to equation (26)

$$\underline{R} = \lim_{\Delta\tau\to o} \sum_j \Psi(j\Delta\tau)\underline{B}(\Delta\tau) \quad . \tag{29}$$

Under the assumption that equation (27) is the valid distribution for $\underline{B}(\Delta\tau)$, $\underline{R}$ becomes the sum of a series of independent normal random variables. Therefore, the distribution of $\Psi(j\Delta\tau)\ \underline{B}(\Delta\tau)$ is

$$f(\underline{R}) = \frac{1}{\left[\ 4\pi D \int_o^t \Psi^2(\varepsilon)d\varepsilon\right]^{1/2}} \exp\left[\ -\frac{1}{4}|\ \underline{R}\ |^2 \Big/ \underline{D} \int_o^t \Psi^2(\varepsilon)d\varepsilon\right] \tag{31}$$

since $\lim_{\Delta\tau\to o} \sum_j \Psi^2(j\Delta\tau)\Delta\tau = \int_o^t \Psi^2(\varepsilon)d\varepsilon$.

Equation (31) is valid only if the assumed distribution for $B(\Delta\tau)$ given by equation (27) is true. If the use of equations (31) and (27) yields a Gaussian distribution for the field free case, their use will be justified for other functions $\Psi(\varepsilon)$.

Returning to equation (24),

$$\Psi(\varepsilon) = \frac{1}{\beta}\left(1 - e^{-\beta(t-\xi)}\right) , \tag{32}$$

and the integral for $\Psi^2(\varepsilon)$ becomes

$$\int_o^t \Psi^2(\varepsilon)d\varepsilon = \frac{1}{2\beta^3}\left[\ 2\beta t - 3 + 4e^{-\beta t} - e^{-2\beta t}\right] \quad . \tag{33}$$

For large t,

$$\int_0^t \psi^2(\varepsilon)d\varepsilon \cong \frac{t}{\beta^2} \quad . \tag{34}$$

Therefore, using equation (31),

$$f\ [\underline{X}(t)] = \frac{1}{\left[2\left(\frac{2\underline{D}t}{\beta^2}\right)\right]^{1/2}} \exp\left[-\frac{1}{2}\,|\,\underline{X}(t)\,|^2 \Big/ \left(\frac{2\underline{D}t}{\beta^2}\right)\right] \quad . \tag{35}$$

Equation (35) is a Gaussian distribution with a variance equal to $\frac{2\underline{D}t}{\beta^2}$, justifying equations (27) and (31).

The representations in equations (27) and (31) are similar to that used by Chandrasekhar for Brownian motion (4). However, in Brownian motion, the velocities of the particles approached a Maxwellian distribution for large t whereas in our case, the displacements of the particles approached a Gaussian distribution for large t. It should also be noted that the variance given for $\underline{X}(t)$ by equation (35) is the same as the variance derived earlier in equation (8) which lends further credence to equations (27) and (31).

The Development of the Partial Differential Equation for the Case of a Gravity Force Field

In the case of a discrete particle in the presence of a gravity force field, equation (1) is the stochastic differential equation describing the particle motion. In this analysis, it will be assumed that the gravitational force field is along the x_3 axis. The solution

to equation (1) is

$$\underline{v}(t) = \underline{v}_o e^{-\beta t} - \frac{g'}{\beta} [1 - e^{-\beta t}] + e^{-\beta t} \int_o^t e^{\beta\tau} \underline{A}(\tau) d\tau \tag{36}$$

where

$$g' = (1 - \frac{\rho_o}{\rho}) g.$$

Integrating (36) to obtain $\underline{X}(t)$ yields

$$\underline{X}(t) = \frac{\underline{v}_o}{\beta} [1 - e^{-\beta t}] - \frac{g'}{\beta^2} [\beta t + e^{-\beta t} - 1] + \int_o^t \int_o^\tau e^{\beta(\varepsilon - \tau)} \underline{A}(\varepsilon) \underline{A}(\tau) d\varepsilon d\tau \quad . \tag{37}$$

Equation (37) can be further simplified by integration by parts to obtain

$$\underline{X}(t) = \frac{\underline{v}_o}{\beta} [1 - e^{-\beta t}] - \frac{g'}{\beta^2} [\beta t + e^{-\beta t} - 1] + \frac{1}{\beta} \int_o^t \underline{A}(\tau) d\tau - \frac{1}{\beta} e^{-\beta t} \int_o^t e^{\beta\tau} \underline{A}(\tau) d\tau \quad . \tag{38}$$

For large t, the distribution of $\underline{X}(t) - \frac{\underline{v}_o}{\beta} [1 - e^{-\beta t}]$ again approaches that of X(t); thus, equation (38) can be written as

$$\underline{X}(t) + \frac{g'}{\beta^2} [\beta t - 1] = \int_o^t \frac{1}{\beta} [1 - e^{-\beta(t - \varepsilon)}] \underline{A}(\varepsilon) d\varepsilon \quad . \tag{39}$$

Referring to equation (32), $\Psi(\varepsilon)$ for the case of a gravitational force field is

$$\Psi(\varepsilon) = \frac{1}{\beta} [1 - e^{-\beta (t - \varepsilon)}] , \tag{39a}$$

and

$$\int_0^t \psi^2(\varepsilon)d\varepsilon = \frac{1}{2\beta^3}\left[2\beta t - 3 + 4e^{-\beta t} - e^{-2\beta t}\right] \tag{39b}$$

$$\cong \frac{t}{\beta^2}$$

for large t. The probability density function for

$$\underline{G} = \underline{X}(t) + \frac{g'}{\beta^2}\left[\beta t - 1\right] \tag{40}$$

becomes upon using equation (31)

$$f(\underline{G}) = \frac{1}{\left[4\pi \frac{\underline{D}t}{\beta^2}\right]^{1/2}} \exp\left[-\frac{1}{2}\,|\,\underline{G}\,|^2 \Big/ \frac{2\underline{D}t}{\beta^2}\right] . \tag{41}$$

$\underline{X}(t)$ is therefore a normal process with a mean

$$\overline{\underline{X}(t)} = -\frac{g'}{\beta}\left[\beta t - 1\right]$$

and a variance of $2\underline{D}t/\beta^2$. The characteristic function for $\underline{X}(t)$ is

$$\Phi_{\underline{x}}(\underline{\xi}) = \exp\left[-i\xi_3 \frac{g'}{\beta^2}(\beta t - 1) - \frac{1}{2}\xi_i \xi_j \frac{2\underline{D}t}{\beta^2}\right] . \tag{42}$$

Using conditional probability, the probability distribution for the position of a particle becomes

$$P[\underline{x}(t)] = \int P[\underline{x}(t_o)]\; Q\,[\underline{x}(t) - \underline{x}(t_o)\,|\,\underline{x}(t_o)]\; d\underline{x}_o .$$

By applying the convolution principle and writing the characteristic function as was done in the field free case the characteristic equation for $P\,[\underline{x}(t)]$ becomes

$$\Phi_{\underline{x}}(\underline{\xi}) = \Phi_{\underline{x}_o}(\underline{\xi})\;\Phi_{(\underline{x}-\underline{x}_o)}(\underline{\xi}) . \tag{42a}$$

Substitution of equation (42) for $\Phi_{(\underline{x}-\underline{x}_o)}(\underline{\xi})$ into equation (42a) yields

$$\Phi_{\underline{x}}(\underline{\xi}) = \Phi_{\underline{x}_o}(\underline{\xi}) \exp\left[-i\xi_3 \frac{g'}{\beta^2} (\beta t - 1) - \frac{1}{2} \xi_i \xi_j \frac{2\underline{D}t}{\beta^2} \right] . \tag{43}$$

The inverse transform of equation (43) can be differentiated with respect to time to yield

$$\frac{\partial P[\underline{x}(t)]}{\partial t} = \frac{\partial}{\partial t} \left[-i\xi_3 \frac{g'}{\beta^2} (\beta t - 1) - \frac{1}{2} \xi_i \xi_j \frac{2\underline{D}t}{\beta^2} \right] \left[\frac{1}{8\Pi^3} \iiint \Phi_{\underline{x}_o}(\underline{\xi}) \Phi_{(\underline{x}-\underline{x}_o)}(\underline{\xi}) e^{-i \underline{\xi} \underline{x}} d\underline{\xi} \right] . \tag{44}$$

Since the integral of the right hand side of equation (44) is $P[\underline{x}(t)]$, the expression for the time derivative of $P[\underline{x}(t)]$ is

$$\frac{\partial P[\underline{x}(t)]}{\partial t} = -i\xi_3 \frac{g'}{\beta} \left[P[\underline{x}(t)] \right] - \xi_i \xi_j \frac{\underline{D}}{\beta^2} \left[P[\underline{x}(t)] \right] . \tag{45}$$

Equation (45) can be written as (see Appendix A 1)

$$\frac{\partial P[\underline{x}(t)]}{\partial t} = \frac{\underline{D}}{\beta^2} \frac{\partial P[\underline{x}(t)]}{\partial x_i \partial x_j} + \frac{g'}{\beta} \frac{\partial P[\underline{x}(t)]}{\partial x_3} . \tag{46}$$

As indicated by equation (22), $\frac{\underline{D}}{\beta^2}$ is equal to $u_i' u_j' L_T$; hence,

$$\frac{\partial P[\underline{x}(t)]}{\partial t} = u_i' u_j' L_T \frac{\partial P[\underline{x}(t)]}{\partial x_i \partial x_j} + (1 - \frac{\rho_o}{\rho}) \frac{g}{\beta} \frac{\partial P[\underline{x}(t)]}{\partial x_3} . \tag{47}$$

Equation (47) is the final proposed model for the diffusion of discrete fluid particles in turbulent flow.

In the actual use of equation (47), a problem arises concerning the form of the coefficient β. The derivation assumes that a drag coefficient can be identified with a fluid particle. An investigation of the validity of this assumption is a complete study in itself and was not undertaken in this research. For this report, β will be assumed to be the drag coefficient for a sediment particle, although this poses theoretical questions concerning the particle velocities used in the derivation.

An alternate derivation of equation (47) is possible using a method similar to that of Batchelor (1). It will be assumed that the probability distribution for the displacement of discrete sediment particles in a gravity force field is normal with a non-zero mean. It will be further assumed that the mean displacement at any time Δt can be given by

$$\overline{\underline{X}(\Delta t)} = -\underline{K}\,\Delta t \tag{48}$$

in which $\underline{K}$ is the fall velocity of the fluid particle. Using Batchelor's approach and starting with equation (12), the characteristic equation for displacement is given by

$$\Phi_{(\underline{x}-\underline{x}_o)}(\underline{\xi}) = \exp\left[-i\xi_3\underline{K}t - \frac{\xi_i\xi_j}{2}\,\overline{X_iX_j}\right] . \tag{49}$$

Using the same procedure as outlined earlier in this chapter, the probability of finding a fluid particle at $\underline{x}$ at time t is given as

$$P[\underline{x}(t)] = \frac{1}{8\Pi^3}\iiint\left(\Phi_{\underline{x}_o}(\underline{\xi}) \exp\left[-i\xi_3\underline{K}t - \frac{\xi_i\xi_j}{2}\overline{X_iX_j} \right] e^{-i\,\underline{\xi}\,\underline{x}}d\underline{\xi}\right) . \quad (50)$$

Differentiating equation (50) with respect to time yields

$$\frac{\partial P[\underline{x}(t)]}{\partial t} = \frac{\partial}{\partial t}\left[-i\xi_3\underline{K}t - \frac{\xi_i\xi_j}{2}\overline{X_iX_j} \right] P[\underline{x}(t)]$$

or

$$\frac{\partial P[\underline{x}(t)]}{\partial t} = \mu_{ij}\frac{\partial P[\underline{x}(t)]}{\partial x_i\,\partial x_j} + \underline{K}\frac{\partial P[\underline{x}(t)]}{\partial x_3} . \quad (51)$$

The term μ_{ij} can be defined again by equation (17) using Csanady's analysis.

This final approach is possibly more rigorous than the approach from the Langevin equation since it does not assume a partition of forces acting on a fluid particle. A problem exists over the selection of a suitable value for $\underline{K}$, since the discussion of turbulent diffusion deals with fluid particles. If it is assumed that $\underline{K}$ is given by the fall velocity of a sediment particle in a still medium, the problem of selecting a value for $\underline{K}$ is essentially that of characterizing β since the quantity $(1-\rho_o/\rho)g/\beta$ in equation (47) is the fall velocity of a particle in a still medium with a drag coefficient of β .

Adaptation of the Equation to Two Dimensional Flow

Using cartesian coordinates and noting that the probability of finding a marked fluid particle at point $\underline{x}$ at time t is equal to the

concentration at that point, equation (47) for isotropic flow becomes

$$\frac{\partial c[\underline{x}(t)]}{\partial t} = u_i^2 L_T \nabla^2 c[\underline{x}(t)] + \underline{K} \frac{\partial c[\underline{x}(t)]}{\partial x_3} \qquad (52)$$

in which ∇^2 is the Laplacian operator. For two dimensional flow with the x_1 axis parallel to the flow and the x_2 axis perpendicular to the flow direction along the horizontal plane;

$$\frac{\partial^2 c}{\partial x_2^2} = 0 \quad .$$

The final proposed model for two dimensional isotropic flow is

$$\frac{\partial c(y,z,t)}{\partial t} = u'^2 L_T \left[\frac{\partial^2 c(y,z,t)}{\partial y^2} + \frac{\partial^2 c(y,z,t)}{\partial z^2} \right] +$$

$$\underline{K} \frac{\partial c(y,z,t)}{\partial z} \quad , \qquad (53)$$

in which z is the x_3 coordinate, y is the X_1 coordinate, and u'^2 is the mean square turbulent fluid velocity.

CHAPTER IV

EXPERIMENTAL PROCEDURES

The experimental verification of the proposed mathematical model was carried out in a recirculating research flume. Glass beads in the silt size range were used as sediment. Tap water was used as the fluid. Concentrations of sediment were determined by gravimetric sampling. The turbulence characteristics were measured with a hot-film anemometer and a random-signal correlator. Table 1 shows the hydraulic data and glass bead size for the various tests.

Description of the Flume and Materials

Research Flume. The apparatus used for the study was a 40-ft. recirculating flume with a channel 12 in. wide and 12 in. deep (see Figures 2 and 3). The sides of the channel were constructed of Lucite for ease of visual observation. The slope of the channel was adjustable by means of worm-type jacks located near the inlet. In this research, the slope was maintained at 0.001 ft. per sec. The catchment tank and the inlet section to the flume were constructed so that fluid separation would not occur and all sediment leaving the exit of the channel would be returned to the entrance by the return pipes. The return pipes had an inside diameter of four inches and the return flow was pumped by a slurry pump powered by a variable speed electric motor. The flow rate was controlled entirely by the motor speed, eliminating buildup of sediment due to valves in the return pipes.

TABLE 1

HYDRAULIC PARAMETERS FOR THE TESTS

Run No.	Depth of Flow D_f ft.	Flow Rate Q cfs	Rainfall Condition	Bead Size No.	Bead Diameter d inches	Mean Velocity U_m fps	Shear Velocity $\sqrt{gD_fS}$ fps	Approximate Reynolds No. R
1A High	0.5	0.735	No	660	.0020	1.45	.013	70,000
1B High	0.5	0.735 + rain	Yes	660	.0020	----	----	------
1A Low	0.5	0.667	No	660	.0020	1.34	.013	65,000
1B Low	0.5	0.667 + rain	Yes	660	.0020	----	----	------
2A High	0.3	0.336	No	380	.0011	1.13	.010	35,000
2B High	0.3	0.336 + rain	Yes	380	.0011	----	----	------
2A Low	0.3	0.307	No	380	.0011	1.03	.010	30,000
2B Low	0.3	0.307 + rain	Yes	380	.0011	----	----	------

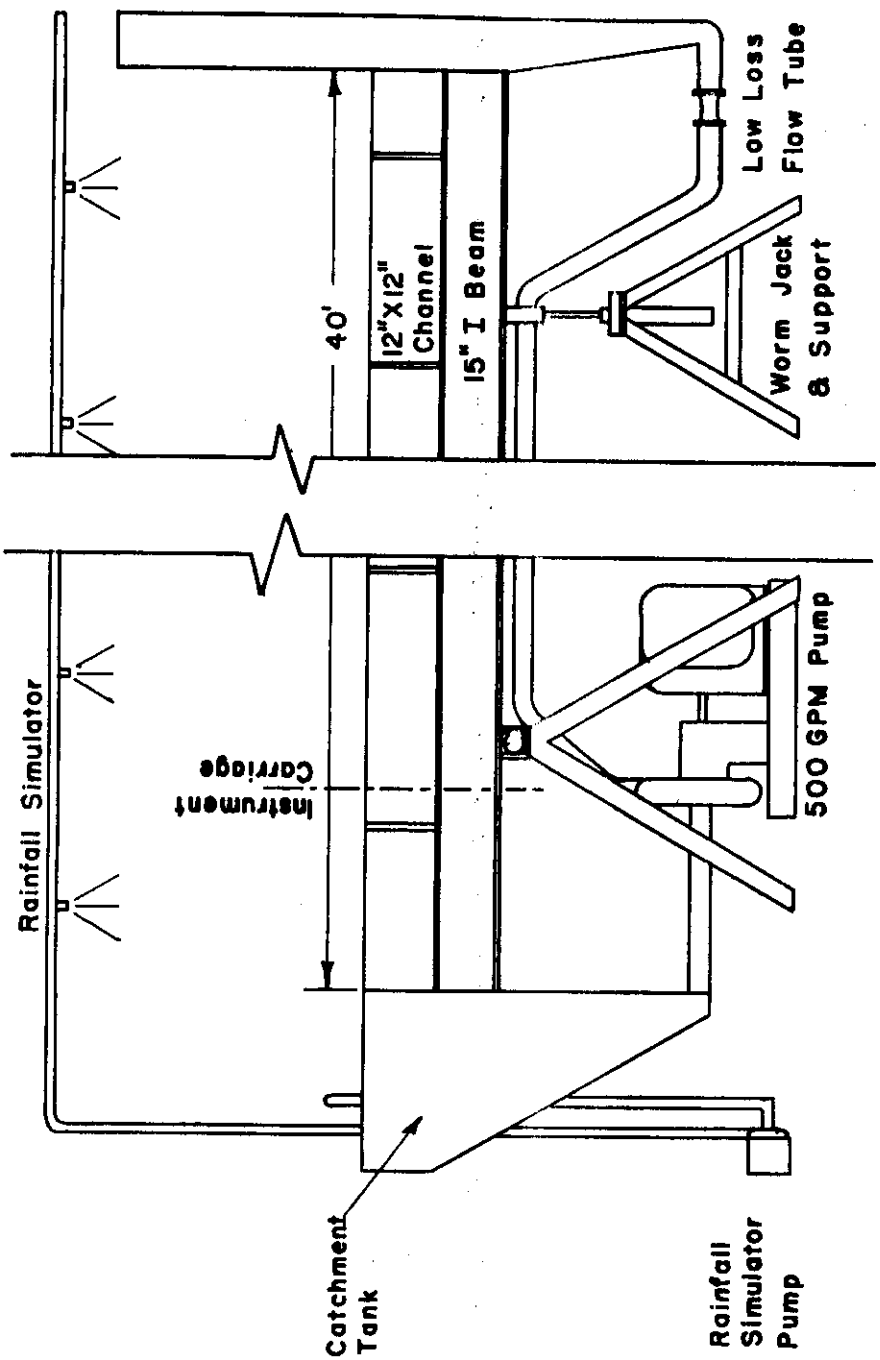

Figure 2. Schematic of Research Flume

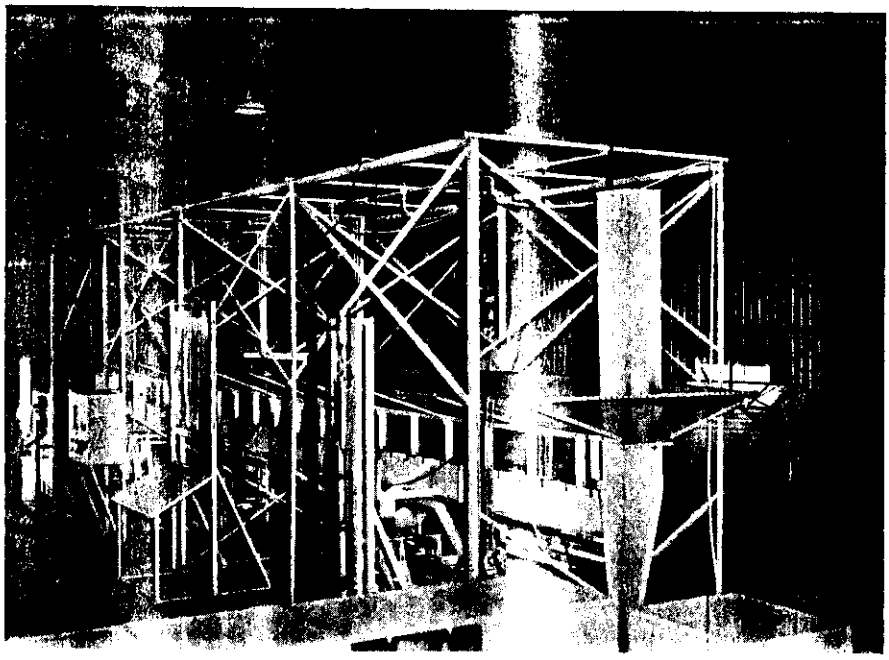

Figure 3. Overall View of Research Flume

The flow rate was measured by a low-loss flow tube connected to a vertical manometer. A manometer fluid of 1.75 specific gravity was used for low flow rates and mercury was used for high flow rates. Since velocity profiles were measured in the flume itself, the only use made of the flow rate determined from the flow tube was to establish flow conditions for each test.

All measurements were made at a test section 5 ft. from the outlet of the channel. An instrument carriage located at this section allowed lateral and vertical movement of all probes.

Simulated rainfall was superimposed on the surface of the flow by Spraying Systems V-jet 80100 nozzles located 8 ft. above the channel surface on 5 ft. centers. This configuration was used by Glass (7) and was recommended by Meyer in 1958 in a study of rainfall simulation (13). The rainfall intensity was held constant throughout the test by maintaining a constant pressure on the nozzles. Figure 4 shows the isolines of rainfall intensity in the channel indicating a fairly uniform distribution.

Materials. As previously mentioned, the fluid used was tap water. In most previous studies involving hot film anemometry, distilled deionized water was used due to its uniformity of heat transfer and due to the problem of air bubbles collecting on the sensor. It was considered desirable in this study to extend the range of uses of hot film anemometry to tap water. The results seemed to indicate that hot film anemometers can be used in tap

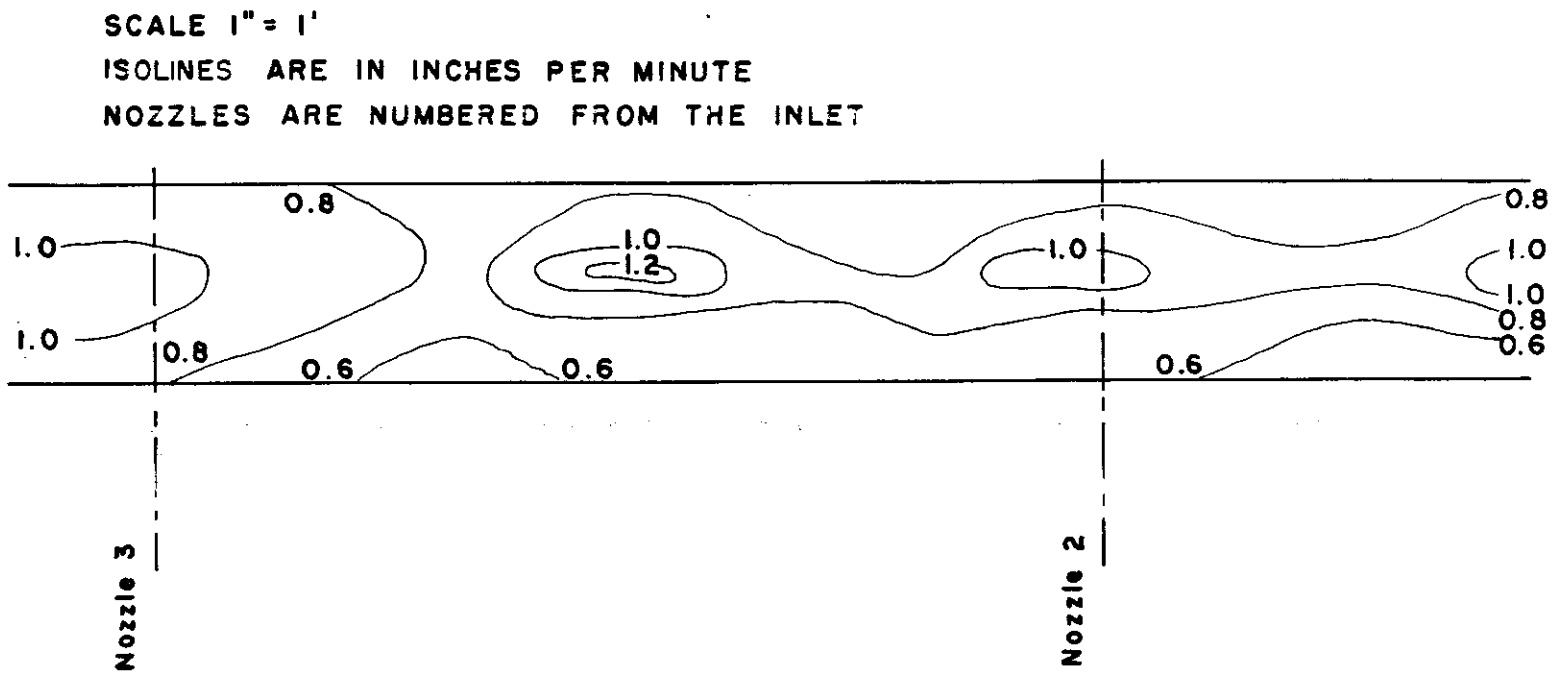

Figure 4. Isolines of Rainfall on the Water Surface

water if proper precautions are taken.

The sediment used in the study was "Superbrite" glass beads manufactured by Minnesota Mining and Manufacturing Company. The properties of the beads are given in Table 2 based on the manufacturer's specifications. When dry, the beads have a texture resembling that of ordinary face powder. Figure 5 shows a photograph of the glass beads.

Turbulence Measurements

Hot-Film Anemometer. The turbulent velocity signal was obtained by using a DISA 55A01 Anemometer with a Thermo-Systems, Inc. (TSI) quartz coated cylindrical film probe (see Figure 6). The anemometer has both bridge D.C. and RMS voltage meters. In order to match the probe with the anemometer, a power booster manufactured by DISA was used. The basic fundamentals of hot-film anemometry are discussed by Hinze and will not be covered in this report (9). Sediment was not introduced into the water during the turbulence measurements to minimize probe damage.

The mean velocity profile was measured by a pitot tube with the total head and static head connected to a Pace variable reluctance transducer. The transducer modulation and demodulation was accomplished by use of a Pace CD25 transducer indicator (see Figure 7). The output of the transducer was indicated on the CD25 as a percent of full scale static calibration. The published accuracy of the CD25 indicator is 0.1 percent of full scale static deflection. In the

TABLE 2

PHYSICAL PROPERTIES OF GLASS BEADS

Appearance	colorless-approximately spherical
Weight	
Bulk specific gravity	- 1.45 to 1.55
Density	- 2.5 grams/cubic centimeter
Size*	
Bead No. 660	50 microns (.0020 inches)
Bead No. 380	29 microns (.0011 inches)
Size Range**	
Bead No. 660	31 - 69 microns
Bead No. 380	18-40 microns

* Measured microscopically.
**Approximately 90% by weight fall in the size range.

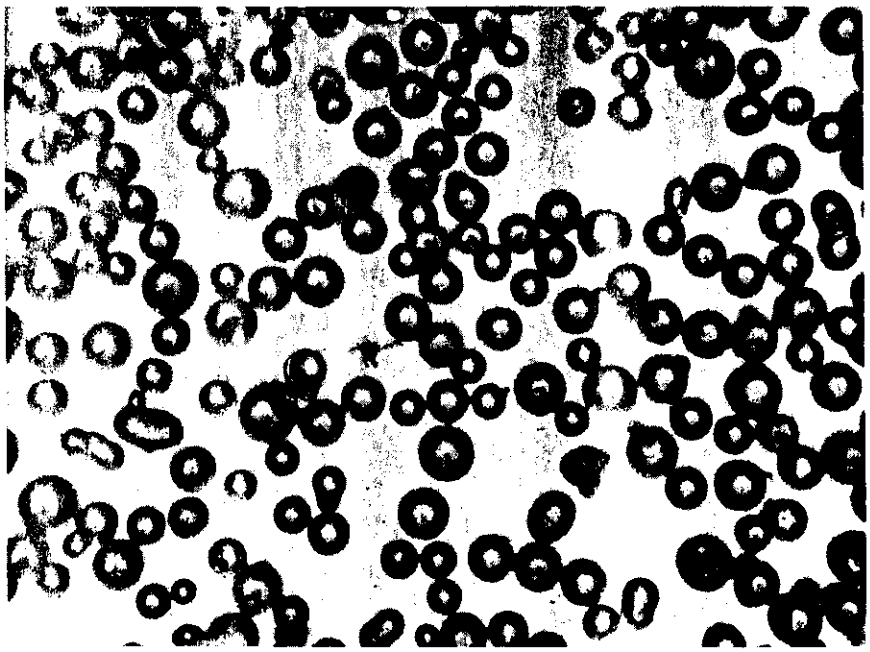

Figure 5. Microphotograph of Glass Beads

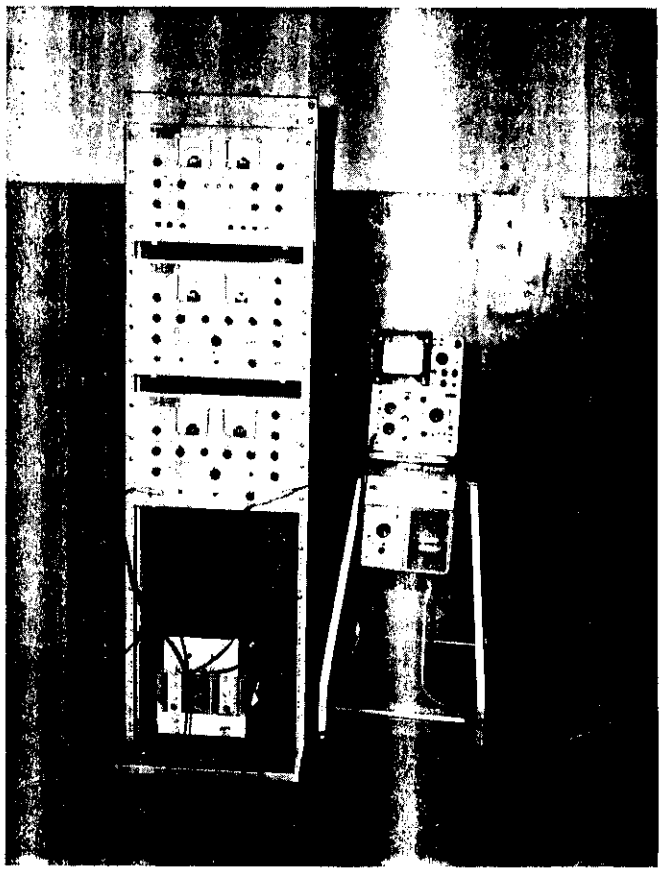

Figure 6. Constant Temperature Anemometer

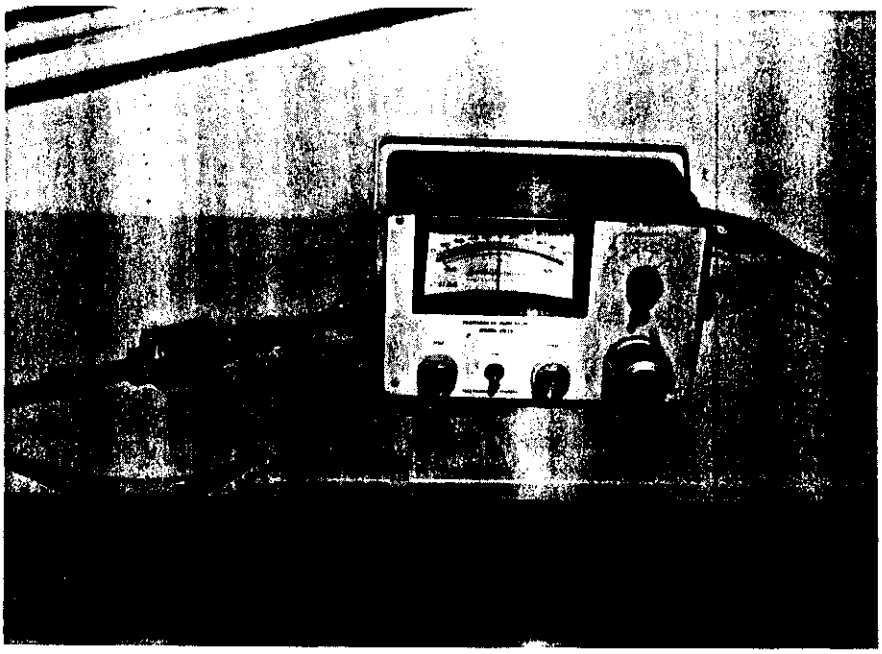

Figure 7. Pressure Transducer and Transducer Indicator

tests run, the output was found to be linear with a maximum error of 2 percent.

Calibration. Hinze states that the heat transfer characteristics between a hot-film probe and fluid flow depend on the geometry of the sensor, the heat conducting characteristics of the fluid, the mean velocity of the fluid, and the temperature difference between the probe and sensor (9). A constant temperature difference is maintained by operating the anemometer so that the resistance of the sensor is at some fixed ratio to its resistance measured at the fluid temperature. This ratio is known as the overheat ratio.

To calibrate the probe, use is made of King's law which is generally stated for hot-film anemometers as

$$V^2 = \alpha' + \beta' \sqrt{\bar{U}}$$

in which V is the anemometer bridge D.C. voltage, $\bar{U}$ the temporal mean velocity, and α' and β' are constants. Linear regression was applied to values of V^2 and $\sqrt{\bar{U}}$ obtained during the actual tests to obtain a calibration curve. Each curve is only valid for a given hot-film sensor, fluid, and overheat ratio.

The calibration was accomplished in the flume itself by setting the hot-film probe in series with a pitot tube (see Figures 8 and 9). The mean velocity was determined by the use of the Pace transducer with a full scale deflection set at 0.2 in. of water. This selection of full scale deflection allowed an instrument accuracy of approximately

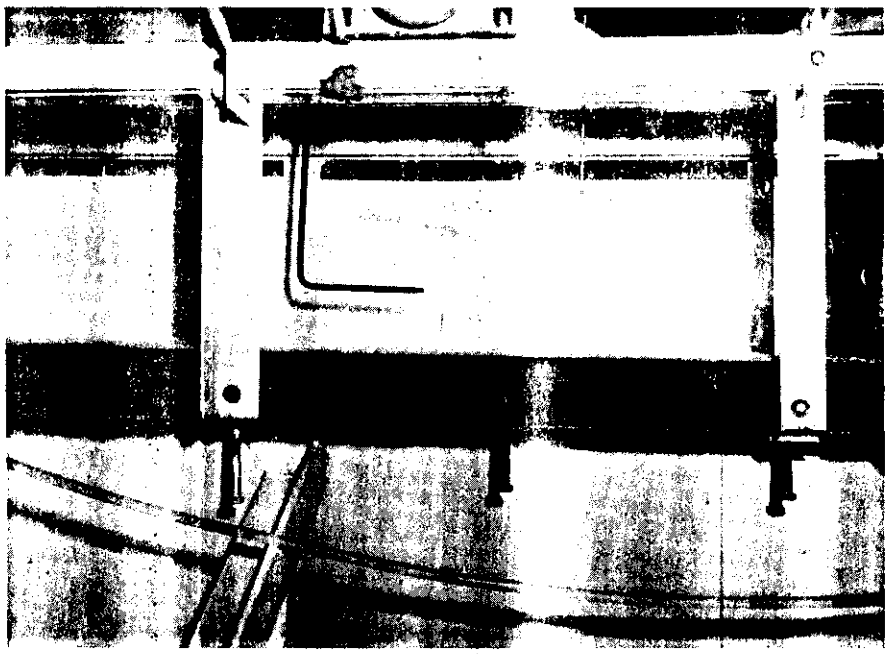

Figure 8. Photograph of Hot-Film Sensor and Pitot Tube in the Flume

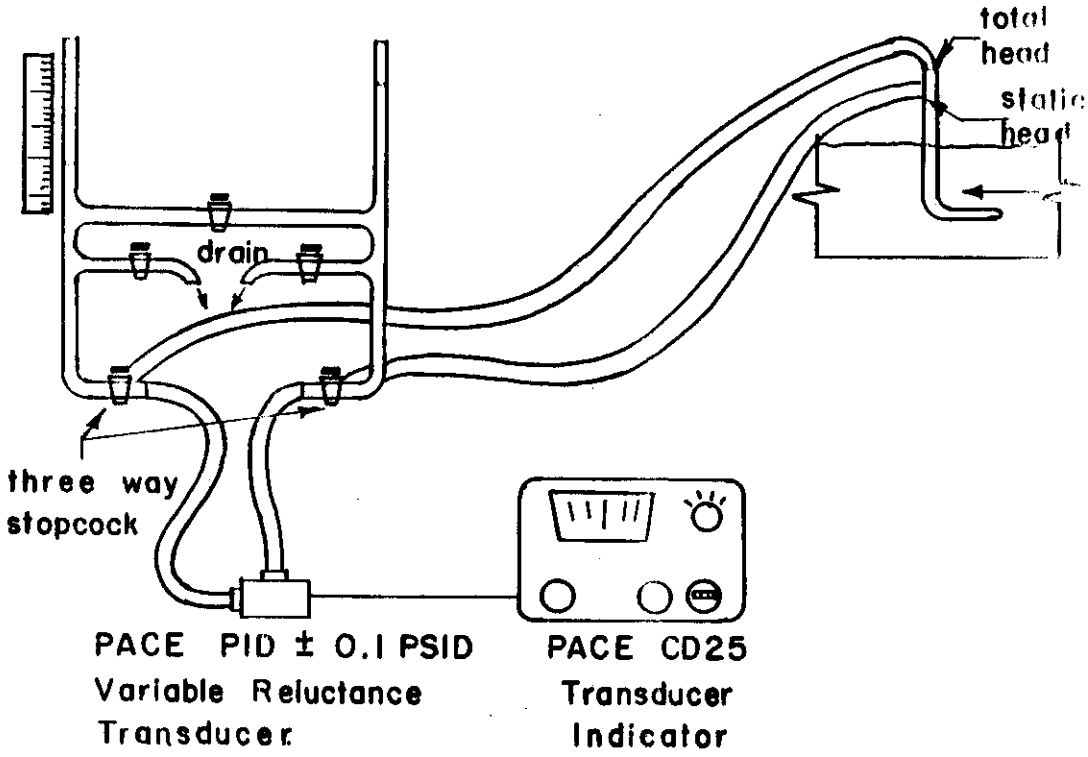

Figure 9. Schematic of Calibration Arrangement

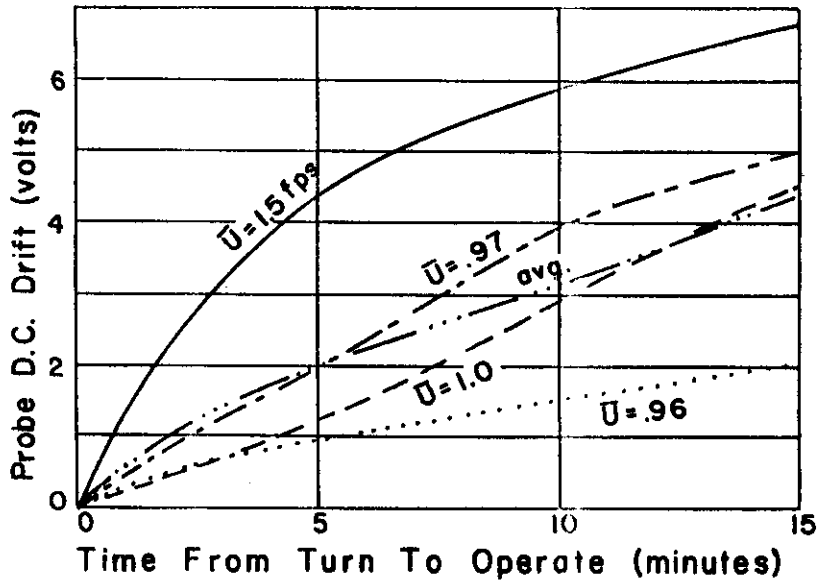

Figure 10. Bridge DC Drift for TSI Cylindrical Sensor

0.025 ft./sec. It should be noted that the sensitivity of the transducer is such that the meter dial fluctuated rather rapidly reducing the accuracy with which the reading could be made. The CD25 indicator has a digital zero suppression meter which allowed the fluctuations to be balanced around some average value; however, the overall accuracy is still estimated by the author to be no better than 0.1 ft./sec.

The anemometer bridge D.C. voltage was taken directly from the D.C. meter on the 55A01 anemometer. A considerable amount of D.C. drift occurred due to collection of debris and air bubbles on the probe. The observed drift for several velocities is shown in Figure 10 and did not appear to be predictable. After trying several procedures, it was found that consistent readings could be obtained if the probe were brushed with a soft artist's brush prior to taking meter readings. The following procedure was used in all tests:

a. The anemometer was switched to a standby position which kept all the tubes warm but did not allow current to flow through the probe.
b. At the standby position, the probe was gently brushed.
c. The anemometer was immediately turned to the operate mode and the initial reading taken of the bridge D.C. voltage and RMS voltage.

It was found that brushing the probe while in the operate mode caused bubbles from the brush to migrate to the probe and

reproducible results could not be obtained.

Figure 11 shows the two calibration curves used in the study. Curve A is for the probe which was used during the tests for depths of 0.5 ft. to determine the RMS velocity profiles. Curve B is for the same probe several days later and was used for the tests for depths of 0.3 ft. to determine RMS velocity profiles. The change in calibration between A and B is probably due to the increased ion content of the water.

Measurements of Time Scale of Turbulence. The time scale for isotropic turbulence is defined in Chapter III as

$$L_T = \int_0^t R(\tau)d\tau$$

in which

$$R(\tau) = \frac{u(t)u(t+\tau)}{u'^2}$$

and u(t) is the turbulent fluid velocity component, u'^2 is the mean square turbulent velocity. To measure L_T, a correlogram was determined by feeding the A.C. output of the anemometer bridge into a Princeton Applied Research Correlator as shown schematically in Figure 12. The correlator performed continuous correlation for 100 points and stored the results on capacitors. The capacitors had a time constant of approximately 20 sec. The delay range used in this test was 1 sec. making the intervals of autocorrelation equal to 0.01 sec. The output of the correlator was filtered and displayed on a Tektronix 564 storage oscilloscope where it was photographed with

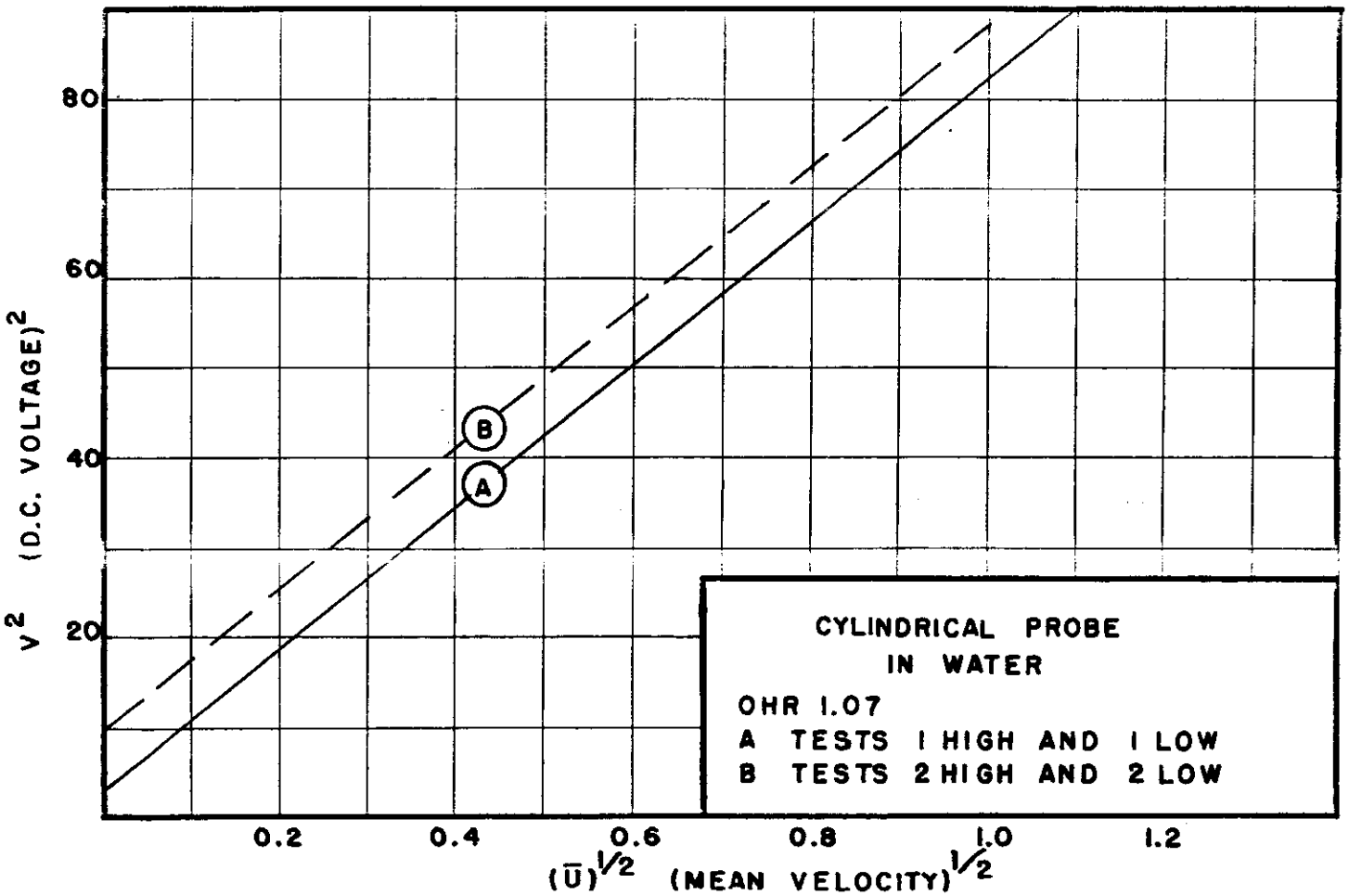
80
60
40
20
V^2 (D.C. VOLTAGE)^2
B
A
CYLINDRICAL PROBE
IN WATER
OHR 1.07
A TESTS 1 HIGH AND 1 LOW
B TESTS 2 HIGH AND 2 LOW
0.2
0.4
0.6
0.8
1.0
1.2
$(\bar{U})^{1/2}$ (MEAN VELOCITY)$^{1/2}$

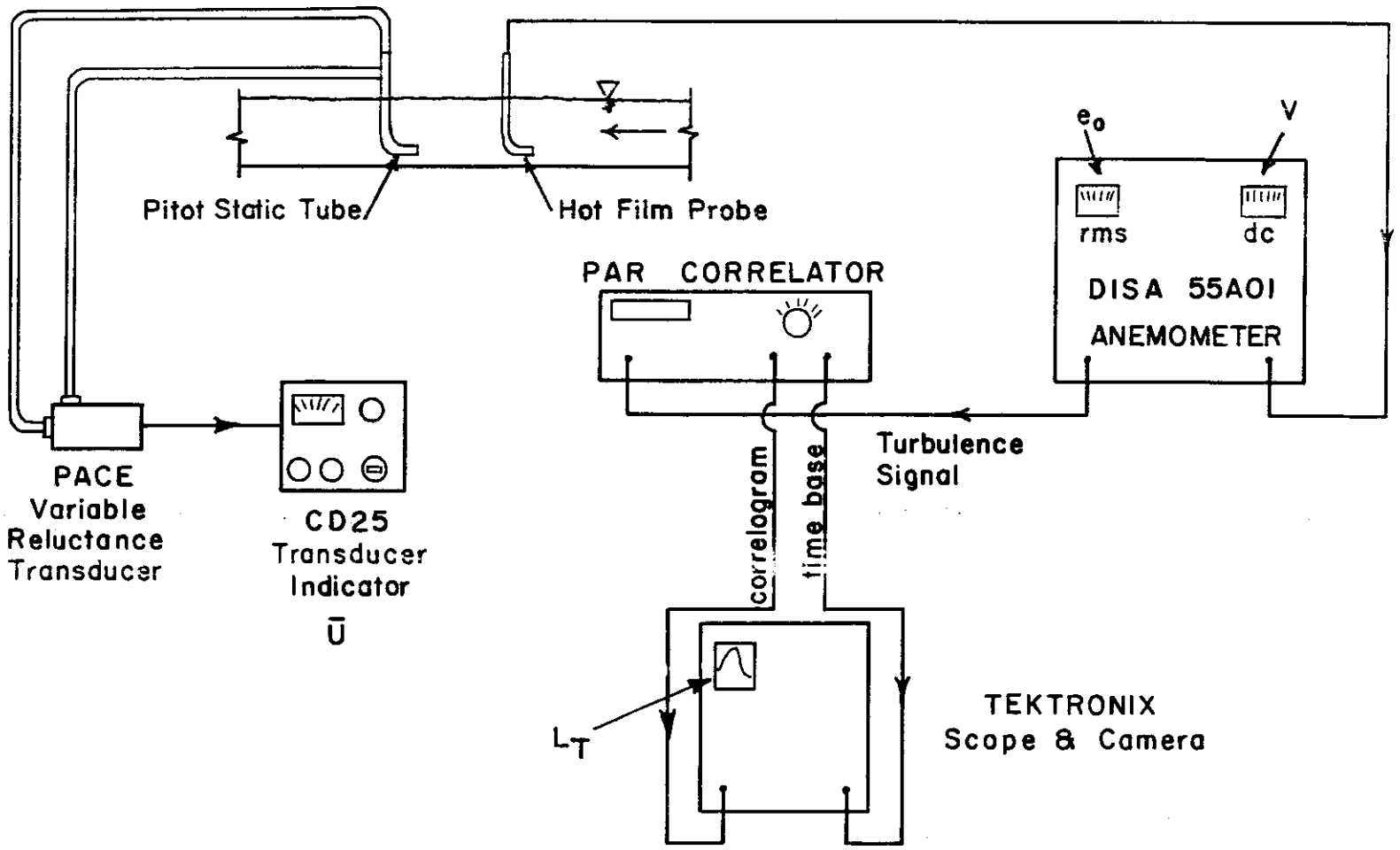

Figure 12. Schematic of Velocity and Turbulence Instrumentation

a Polaroid camera. A typical correlogram is shown in Figure 13.

The following procedure was used in obtaining the length scale of turbulence:

a. With the anemometer in the standby mode, the probe was brushed as mentioned previously.

b. The anemometer was turned to operate and the initial anemometer D.C. voltage reading was taken along with the reading from the Pace transducer indicator providing a continuous calibration check.

c. After 1 min., the output of the correlator was displayed on the oscilloscope and photographed.

Three separate photographs were taken for each relative depth. The value of L_T was determined by manually reading values of $R(\tau)$ from the photograph and using the trapezoidal rule to numerically integrate the area under the curve of $R(\tau)$ versus τ .

Measurement of RMS Velocities. The RMS velocity was determined by multiplying the voltage read from a true RMS voltmeter on a DISA random signal correlator by the derivative of the velocity with respect to the voltage or

$$u' = e_o \frac{d\bar{U}}{dV}$$

in which e_o is the RMS voltage. The time constant on the voltmeter was 20 sec. An error was made in determination of the RMS voltage during the tests in which the length scales of turbulence were measured; therefore, the RMS velocity profiles were determined separately.

Horizontal Scale: 1 cm. = .02 sec.

Vertical Scale: 1 cm. = .2 arbitrary units

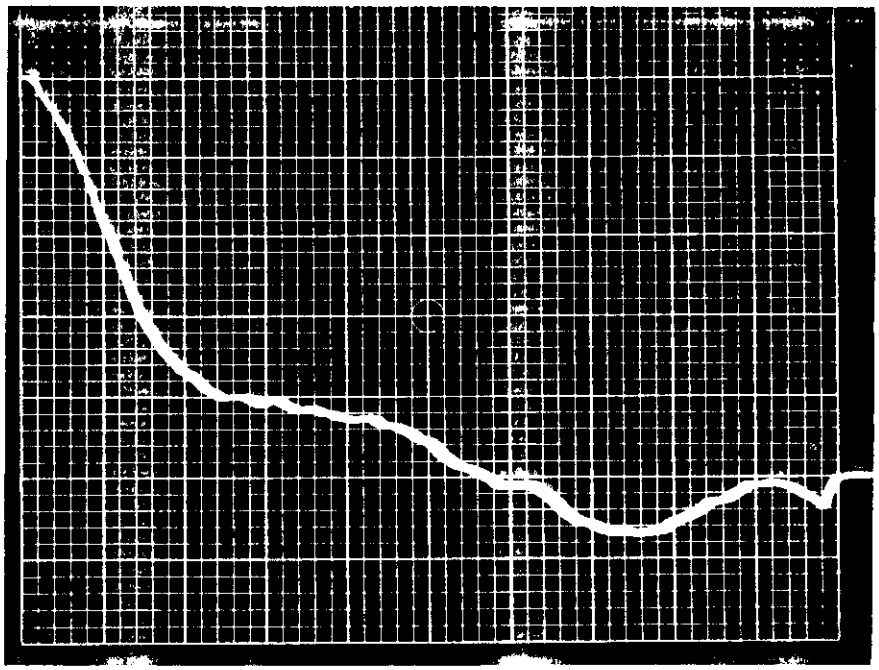

Figure 13. Typical Correlogram as Photographed on the Oscilloscope Display

Sediment Concentration Measurements

Method of Collecting Samples. The concentration profile was measured by siphoning samples of one pint volume from the flow at the instrument section. The siphon tube is shown in Figure 14. The siphoning head was adjusted so that the flow rate into the siphon tube would be approximately that of the mean flow velocity. The inside diameter of the siphon tube was 1/8 in.

The concentration at the inlet was determined by siphoning samples from three, 1/4 in. inside diameter tubes inserted into the inlet section. It was assumed that the concentration was uniform inside the inlet. This was verified by the small variation in the inlet concentrations determined from the separate tubes.

Method of Measuring Concentrations. The sample concentrations were determined by a filtration technique. The weight of the sediment sample plus water was determined by using a Mettler balance with an accuracy of $\pm$0.01 grams. The sample was then poured through filter paper whose published ash content was less than 0.0005 grams. The filter paper and sediment were placed in a furnace and ashed at 550° Centigrade for two hours. The weight of the sediment was determined by use of a Mettler balance with an accuracy of $\pm$0.0001 grams. The minimum weight of sample collected was greater than 0.0200 grams; therefore, the maximum error due to filter paper ash content was 2.5 percent.

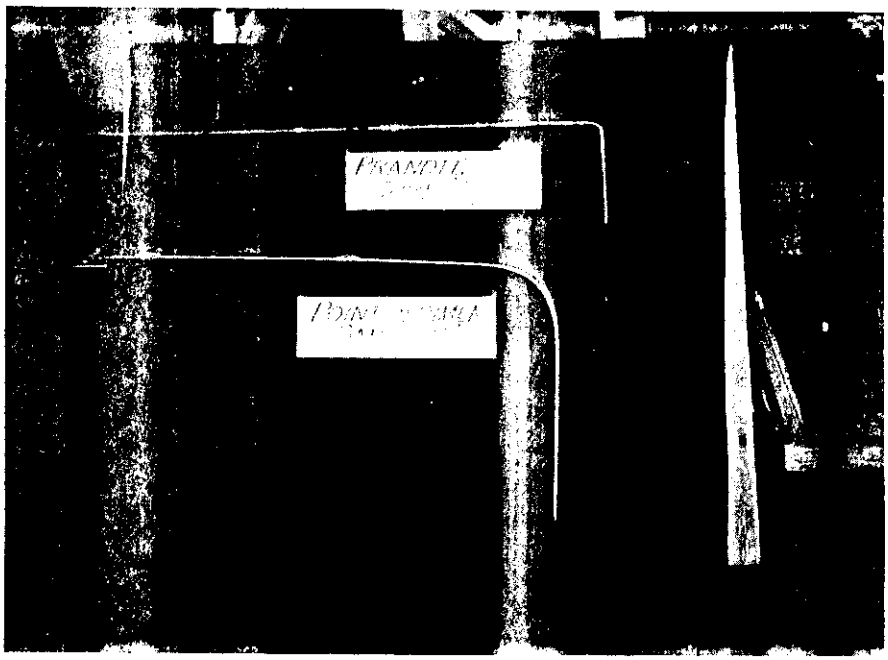

Figure 14. Prandtl Tube and Point Sediment Sampler

CHAPTER V

RESULTS AND DISCUSSION

Investigations involved in the study of turbulent motion of discrete sediment particles as affected by rainfall involve three areas of fluid mechanics in which limited data are available: turbulence characteristics of open channel flow, the effects of superimposed rainfall on the structure of turbulence, and the prediction of sediment profiles from turbulence data. The results of the experimental investigations in each of the three areas will be discussed separately.

Turbulence Characteristics of the Flow

As mentioned in the discussion of experimental procedures in Chapter IV, no sediment was present in the water during the turbulence measurements to minimize probe damage. The bed of the flume in this case was smooth whereas the bed with sediment laden water had dunes as shown in Figure 36 on page 80. The probable effect of the difference in bed roughness is discussed later in this section.

Time Scale of Turbulence. Profiles for the Eulerian time scale of turbulence, as measured by use of the hot-film anemometer and random-signal correlator, are shown in Figures 15 through 18. The data exhibit some scatter and do not seem to follow any general trend with depth for tests without rainfall. The variation for these tests is limited to $\pm$ 0.02 secs. with the exception of two points on Test 1A

in an open channel with a Reynolds number of 66,200. These correlograms compare favorably with those taken in Test 1A Low shown previously in Figure 20 (Reynolds Number = 65,000). From visual observation, however, it appears that the area under Raichlen's curves (the length scale) would be slightly greater than that obtained in Test 1A Low. Rao measured autocorrelation curves for turbulent flow using a capacitance transducer, a DISA random-signal correlator and a AD-YU time delay unit (16). Only four different curves were reported, one at each of four flow conditions, therefore no conclusions concerning the profile could be made. The only correlogram available at comparable conditions to this study was for a Reynolds number of 52,000 which is close to Test 1A Low. The correlogram by Rao was for a relative depth of 0.137 and does not compare favorably with that obtained with the PAR correlator in this study. The correlograms for Test 1A Low show a time for which the correlation becomes zero as being approximately 0.5 to 0.6 sec. (see Figure 20) whereas Rao reports values of 0.02 sec. Rao's tests were made in an artificially roughened channel whereas the measurements reported herein were made in a smooth channel. This could account for the difference; however, rough channels should increase the size of the eddies and thus the time scale. Another possible explanation is the difference in instrumentation.

Root-Mean-Square Velocity Profiles. The accepted method of displaying RMS velocities is to plot relative turbulent intensities

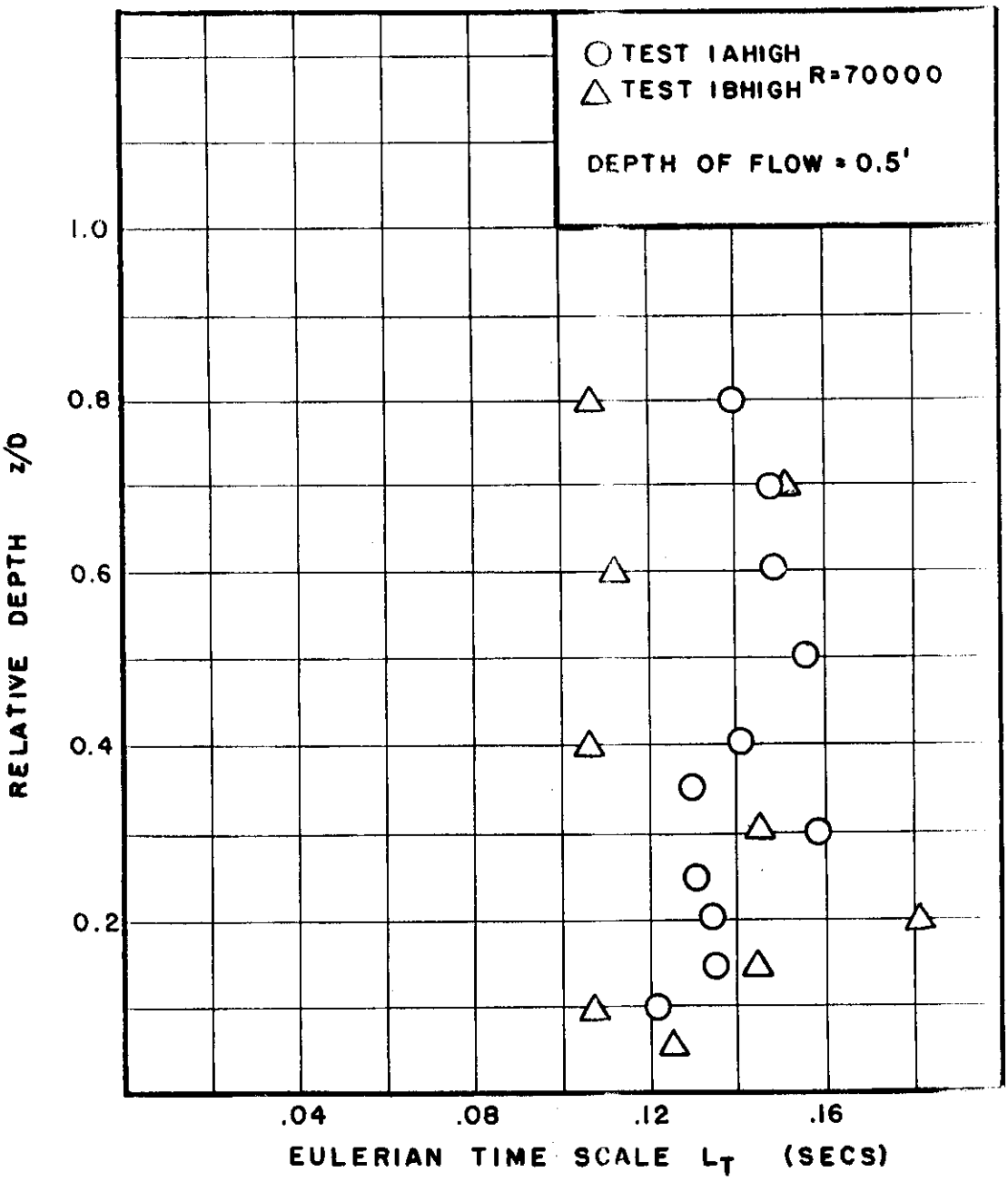

Figure 15. Eulerian Time Scale Profiles for Tests 1A High and 1B High

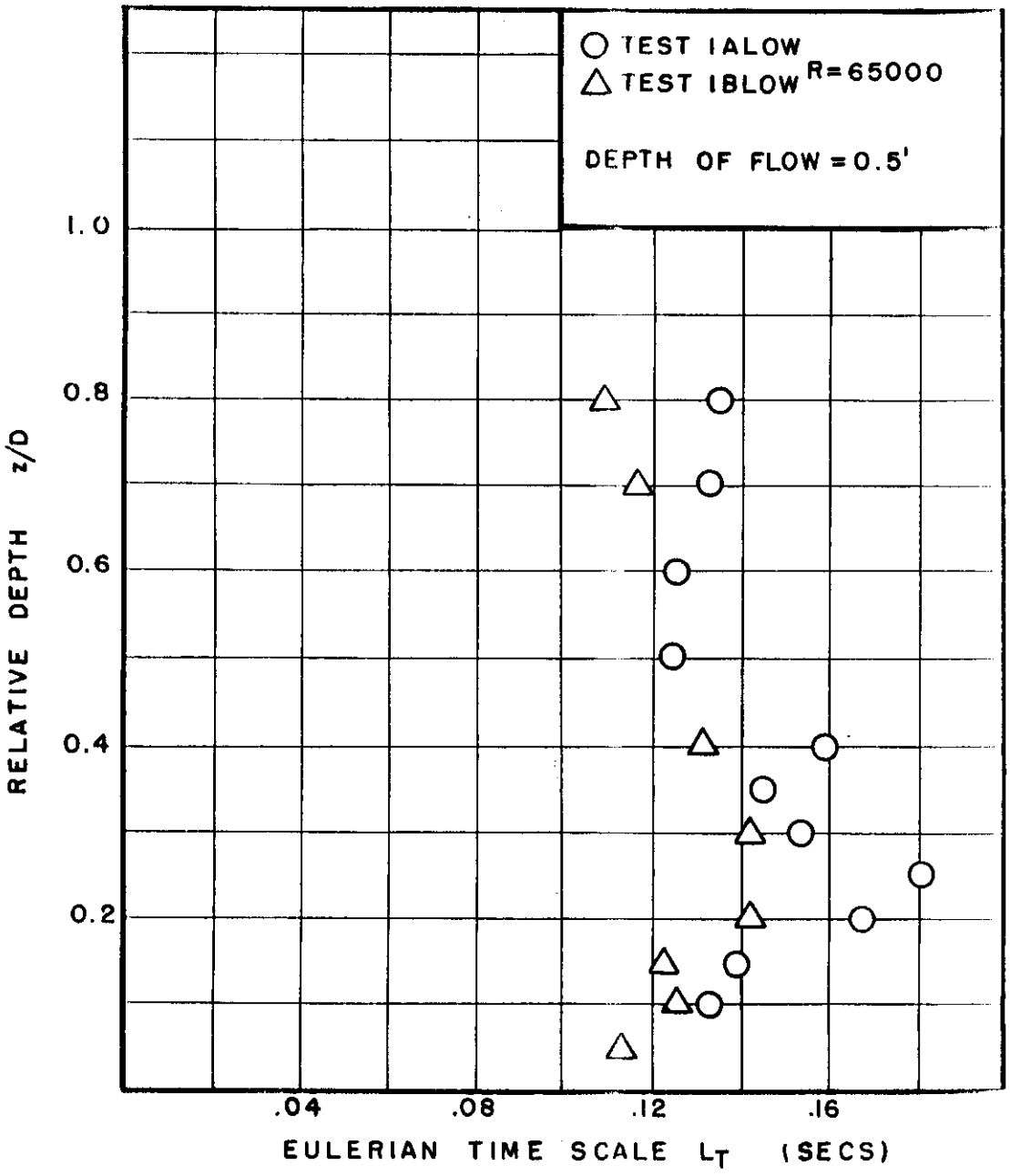

Figure 16. Eulerian Time Scale Profiles for Tests 1A Low and 1B Low

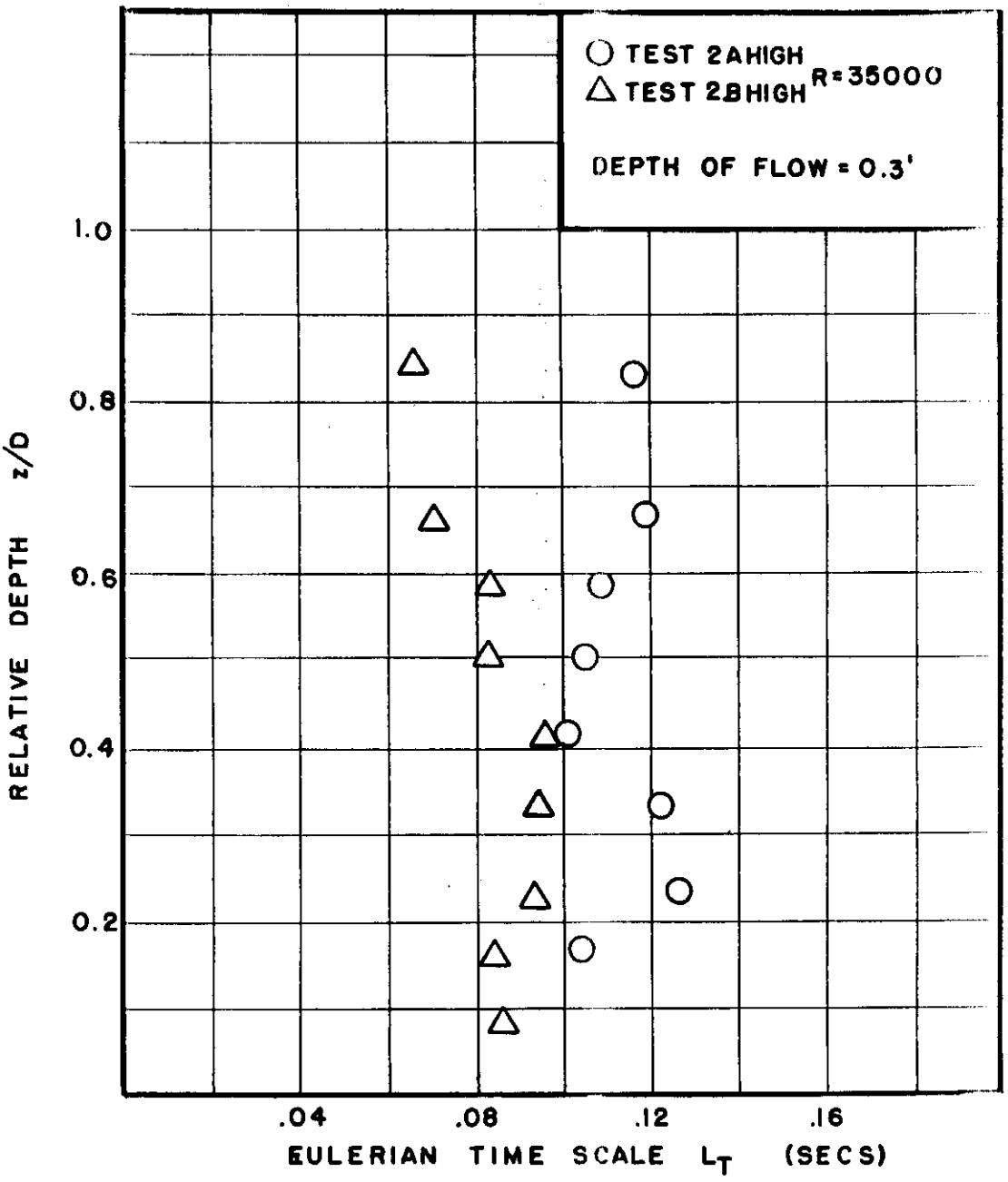

Figure 17. Eulerian Time Scale Profiles for Tests 2A High and 2B High

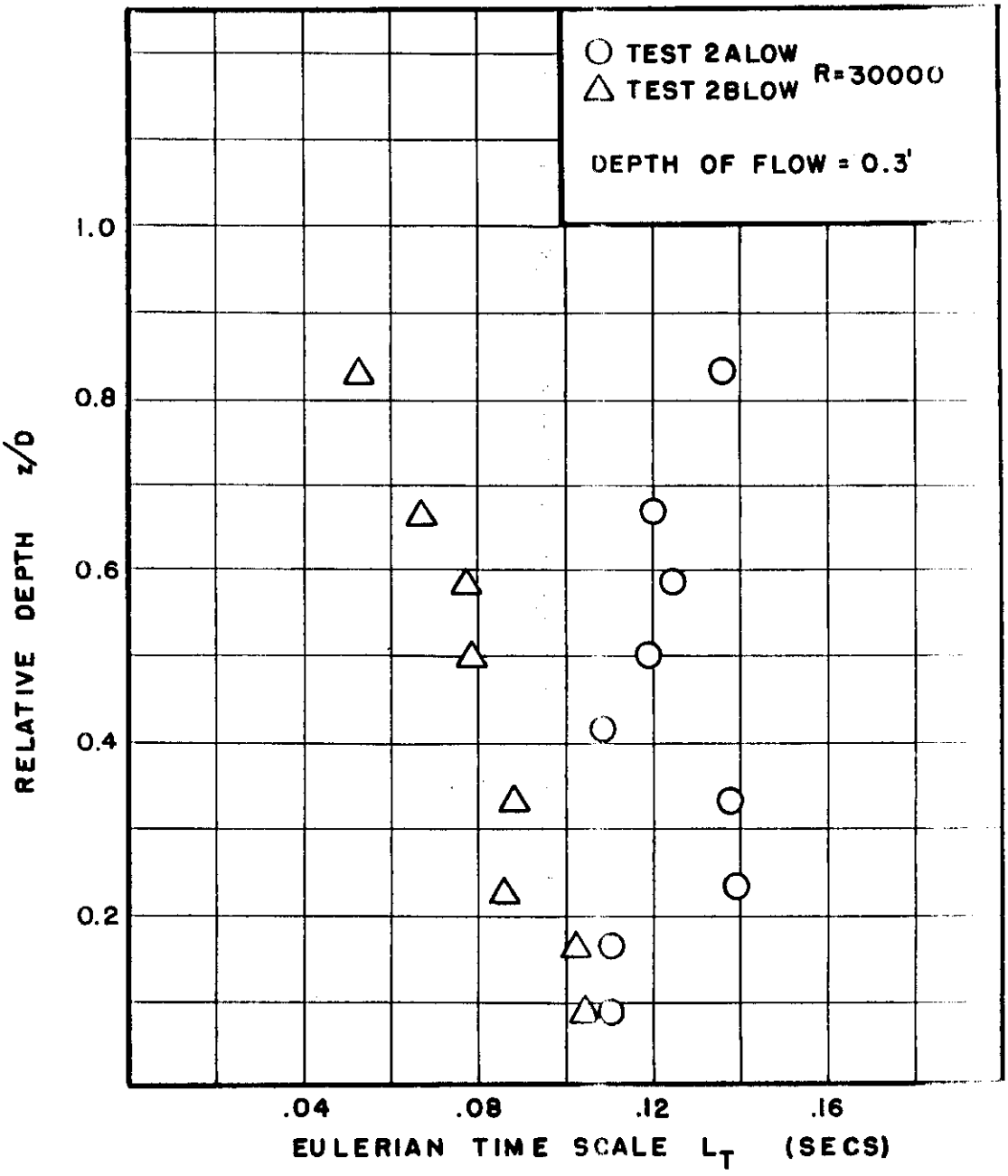

Figure 18. Eulerian Time Scale Profiles for Tests 2A Low and 2B Low

Low. It appears likely that if a trend with depth exists, it is within the ranges of the experimental error.

The correlograms, from which the time scale was determined, are shown in Figures 19 through 22. The variation of the autocorrelation coefficient about zero is evidence of the sampling problem and of the resulting difficulty in determining the time scale.

One of the probable sources of scatter of the points is the problem of ergodicity -- the time average not being equal to the statistical expectation. The effective sample time for the PAR Model 100 correlator is 20 sec. No data are available on the length of time necessary for a good estimate of the correlogram and thus the time scale of turbulence. From the scatter observed in these results, it appears evident that 20 sec. is not sufficient. Raichlen reported similar problems in estimating the correlogram although discrete sampling was used in his data analysis (15). Further research is needed on the sampling problem in turbulence measurements.

The values of the time scale for the depth of 0.5 ft. are greater than those at a depth of 0.3 ft. This leads to the conclusion that the mean eddy size is greater at the deeper flow, a reasonable assumption from mixing length theories.

No profiles of the Eulerian time scale could be found in the literature with which to compare the profiles measured in this study. Raichlen showed one set of correlograms for various relative depths

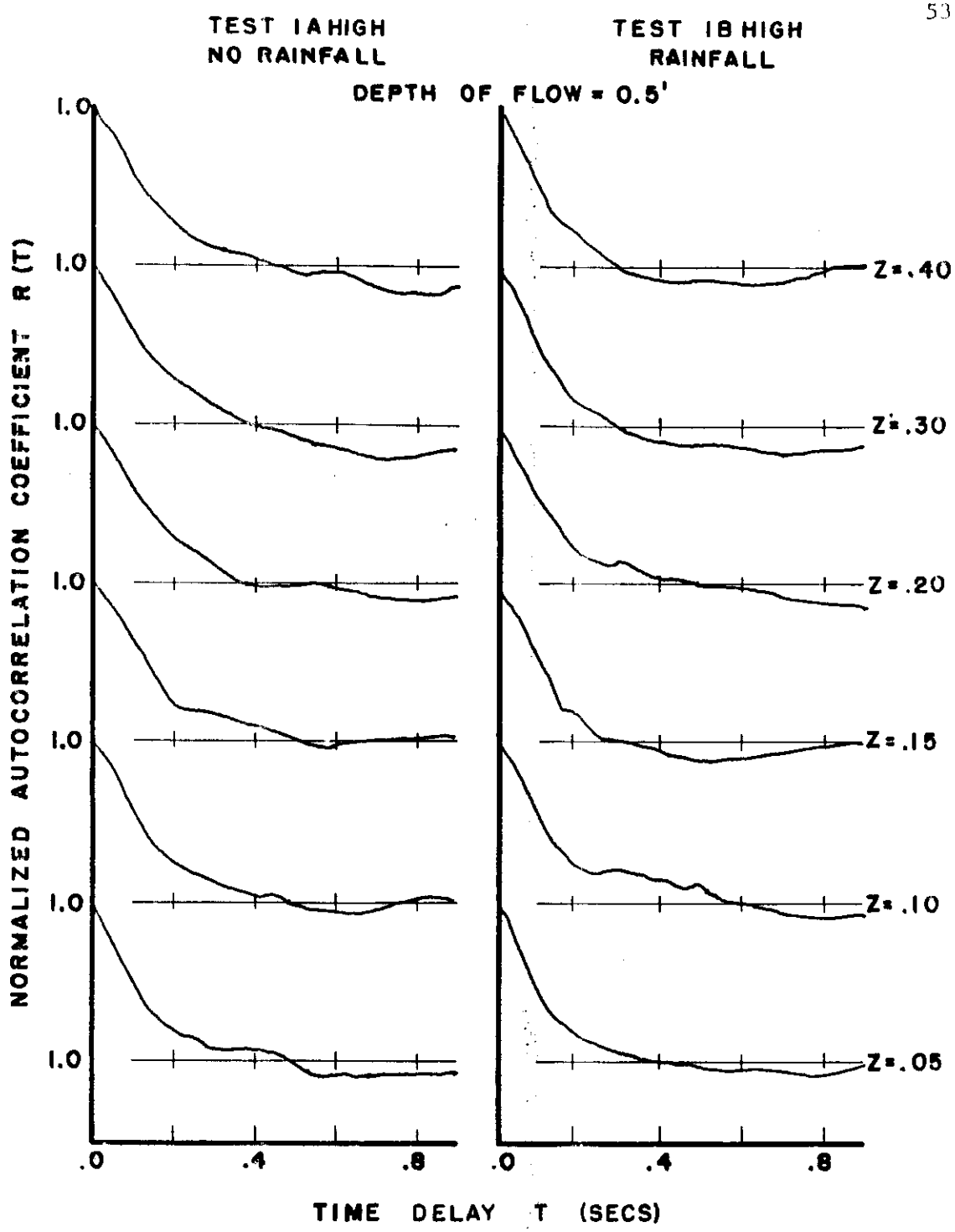

Figure 19. Correlograms for Tests 1A High and 1B High

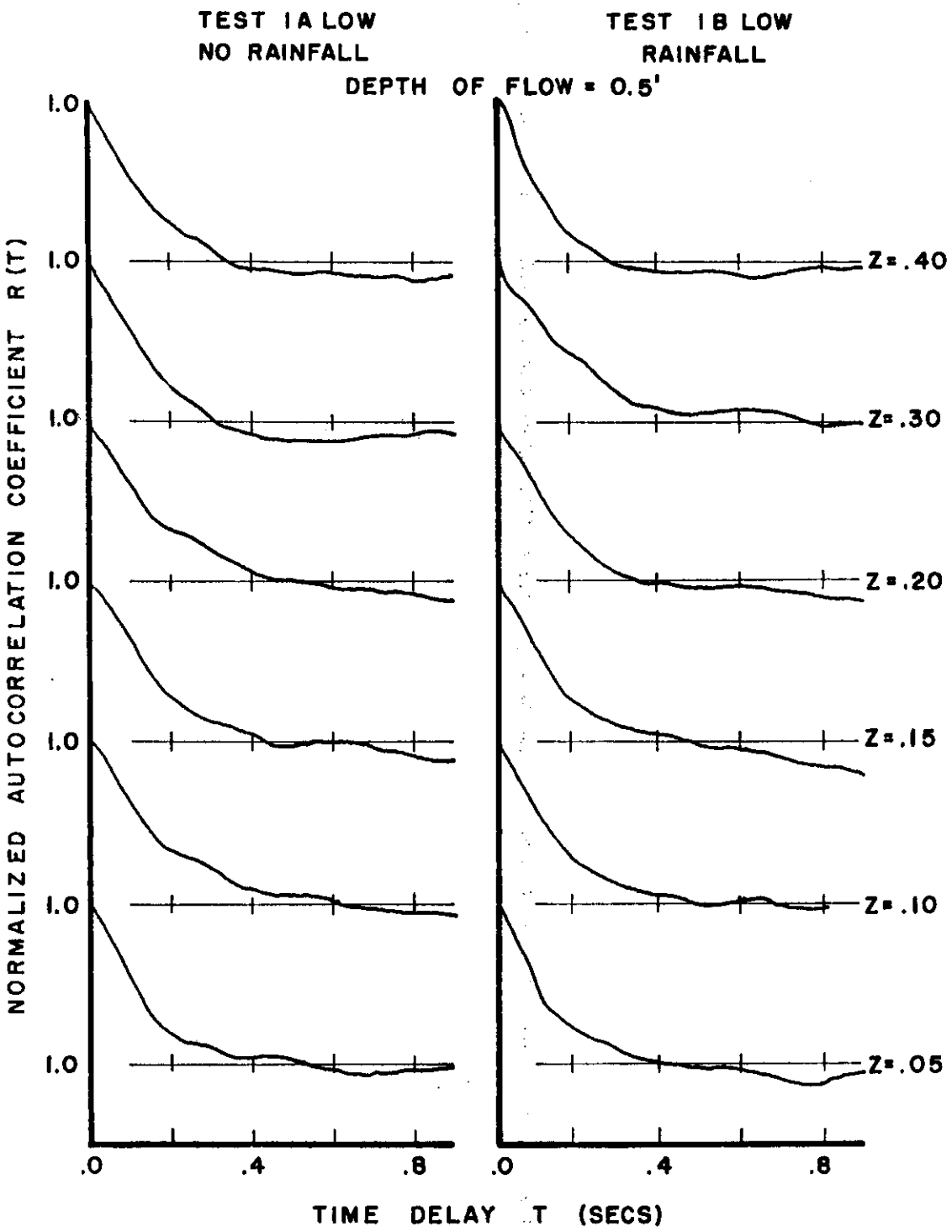

Figure 20. Correlograms for Tests 1A Low and 1B Low

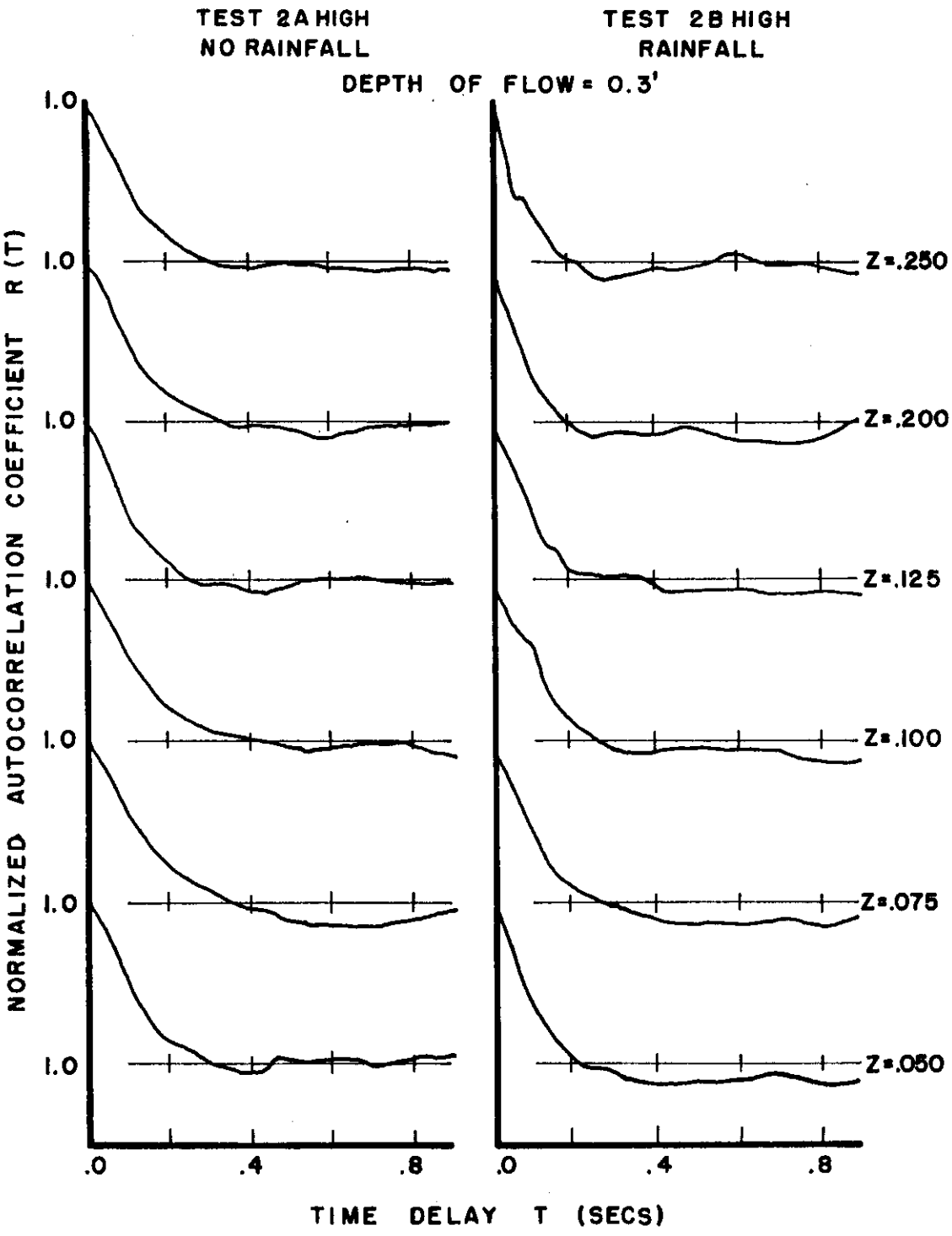

Figure 21. Correlograms for Tests 2A High and 2B High

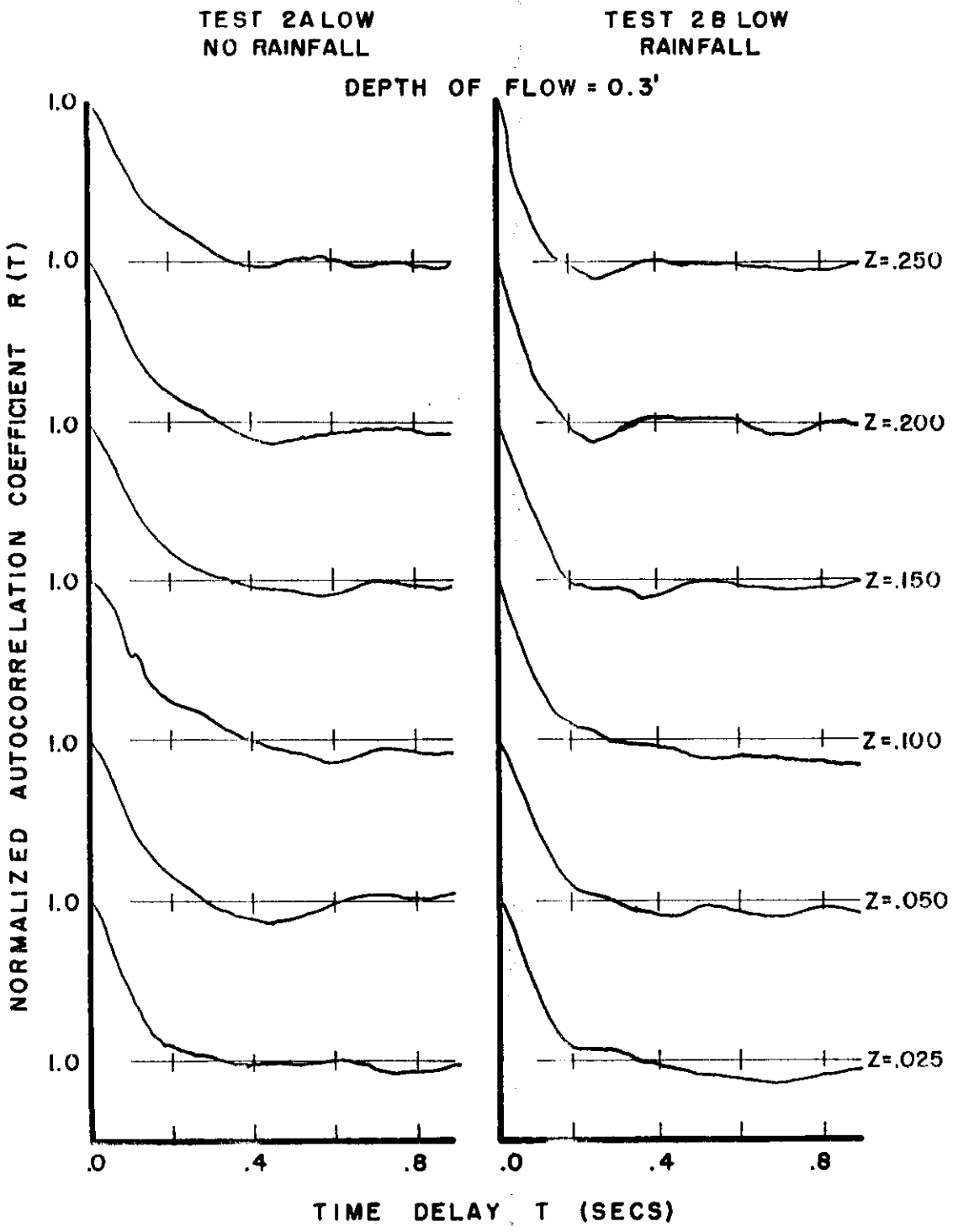

Figure 22. Correlograms for Tests 2A Low and 2B Low

in an open channel with a Reynolds number of 66,200. These correlograms compare favorably with those taken in Test 1A Low shown previously in Figure 20 (Reynolds Number = 65,000). From visual observation, however, it appears that the area under Raichlen's curves (the length scale) would be slightly greater than that obtained in Test 1A Low. Rao measured autocorrelation curves for turbulent flow using a capacitance transducer, a DISA random-signal correlator and a AD-YU time delay unit (16). Only four different curves were reported, one at each of four flow conditions, therefore no conclusions concerning the profile could be made. The only correlogram available at comparable conditions to this study was for a Reynolds number of 52,000 which is close to Test 1A Low. The correlogram by Rao was for a relative depth of 0.137 and does not compare favorably with that obtained with the PAR correlator in this study. The correlograms for Test 1A Low show a time for which the correlation becomes zero as being approximately 0.5 to 0.6 sec. (see Figure 20) whereas Rao reports values of 0.02 sec. Rao's tests were made in an artificially roughened channel whereas the measurements reported herein were made in a smooth channel. This could account for the difference; however, rough channels should increase the size of the eddies and thus the time scale. Another possible explanation is the difference in instrumentation.

Root-Mean-Square Velocity Profiles. The accepted method of displaying RMS velocities is to plot relative turbulent intensities

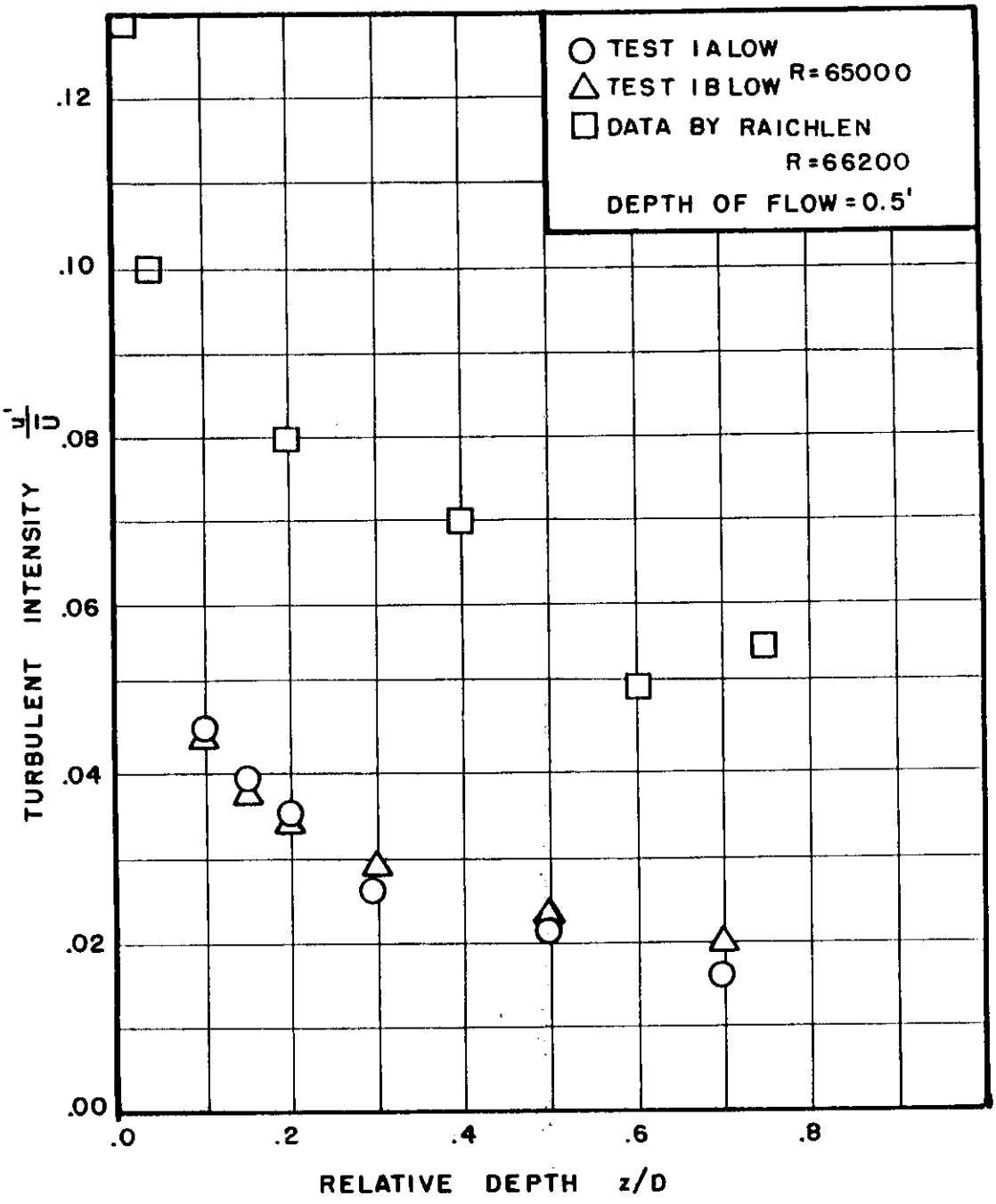

Figure 24. Turbulent Intensity Profiles for Tests 1A Low and 1B Low and Comparison with Raichlen's Data

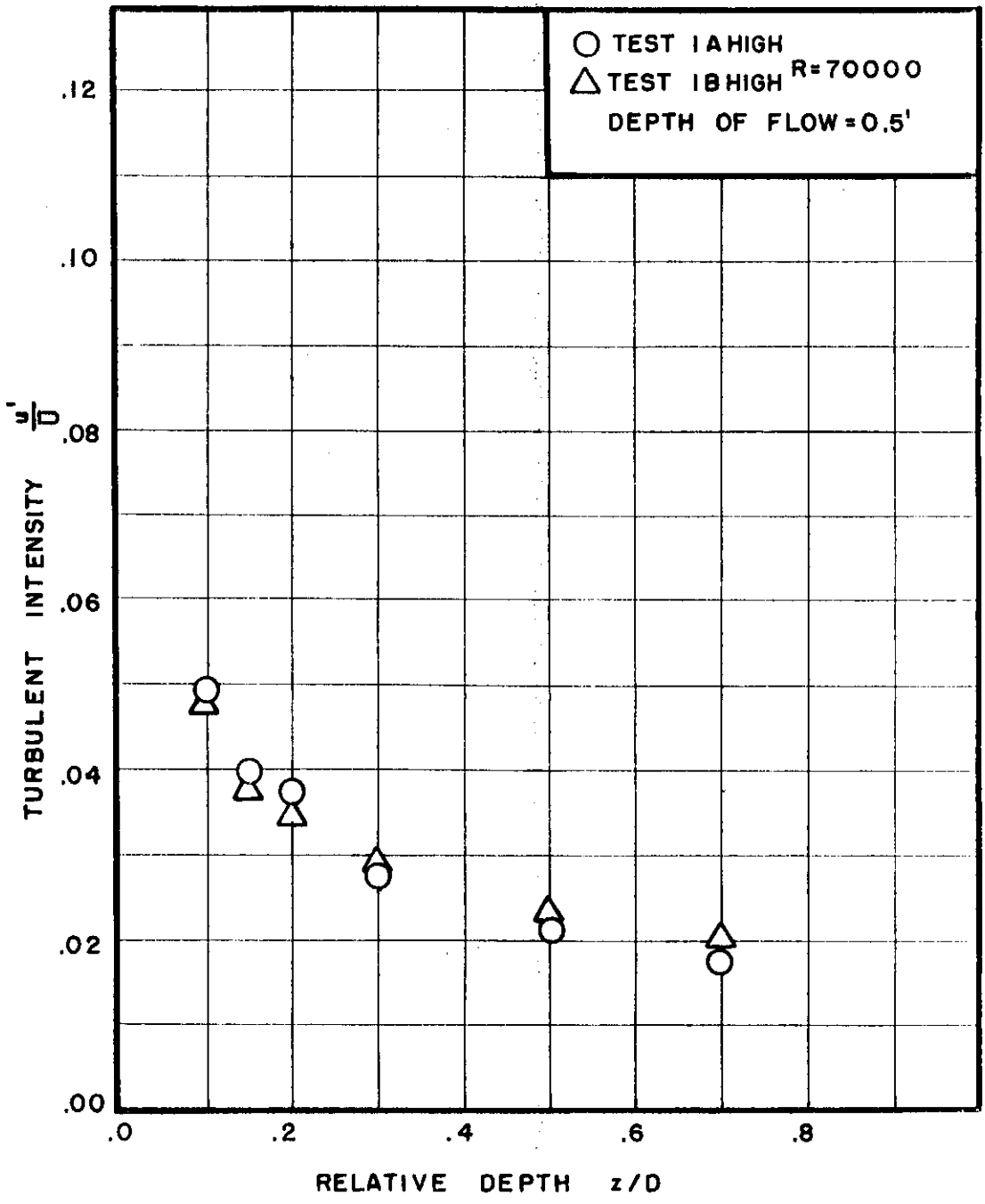

Figure 23. Turbulent Intensity Profiles for Tests 1A High and 1B High

versus relative depth. Relative turbulent intensity is the ratio of the RMS velocity to the temporal mean velocity. Figures 23 to 26 show the plots of turbulent intensity for each flow condition.

By comparing the curves, it is evident that the relative intensity generally decreased with increasing Reynolds number. This is in agreement with data by Laufer in air and data reported by Rao in water (12, 16). In each flow condition, the value of relative intensity decreased from a maximum near the bed to a minimum at the surface. The relative intensities near the water surface were similar for all Reynolds numbers tested, indicating that the Reynolds number effect is most pronounced near the channel bed. This result also agrees with the data published by Rao.

Figure 24 shows a comparison of turbulent intensities for Test 1A Low (Reynolds number = 65,000; shear velocity = 0.013 ft./sec.) to data obtained by Raichlen (Reynolds number = 66,200; shear velocity = 0.0365 ft./sec.). The depth of flow for Raichlen's test was 0.3 ft. and for Test 1A Low, 0.5 ft. In each case the channel bed was painted with epoxy paint and was smooth. Raichlen's values for turbulent intensity were considerably greater than those observed in Test 1A Low. No systematic error could be found in the method of obtaining the RMS velocities reported herein to explain the difference. The voltmeter used on the DISA random-signal correlator has a published accuracy of 2 percent over 50 hz. Energy spectrums by Rao and Raichlen show that a large portion of the turbulent energy comes from frequencies less than 50 hz. which could

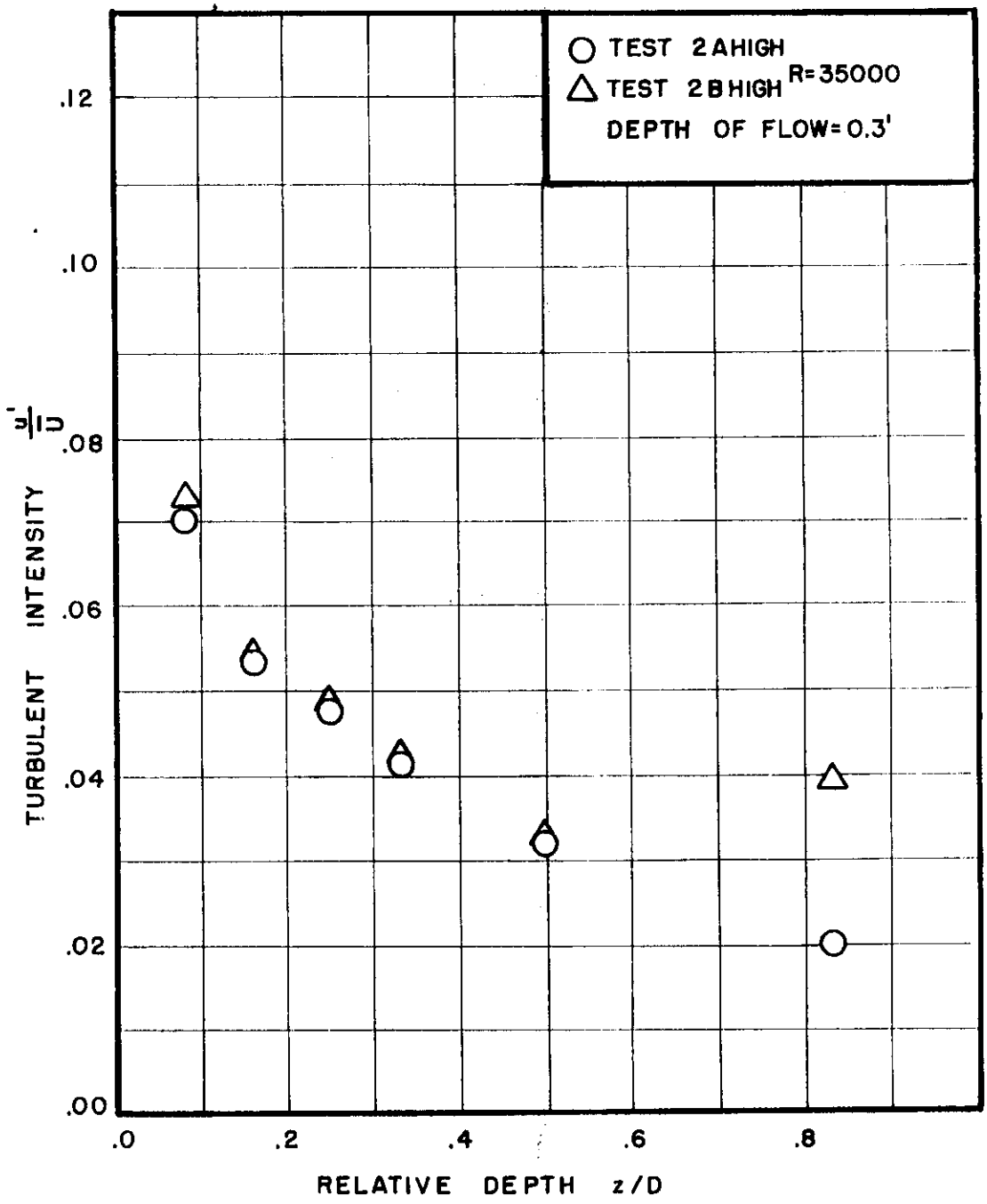

Figure 25. Turbulent Intensity Profiles for Tests 2A High and 2B High

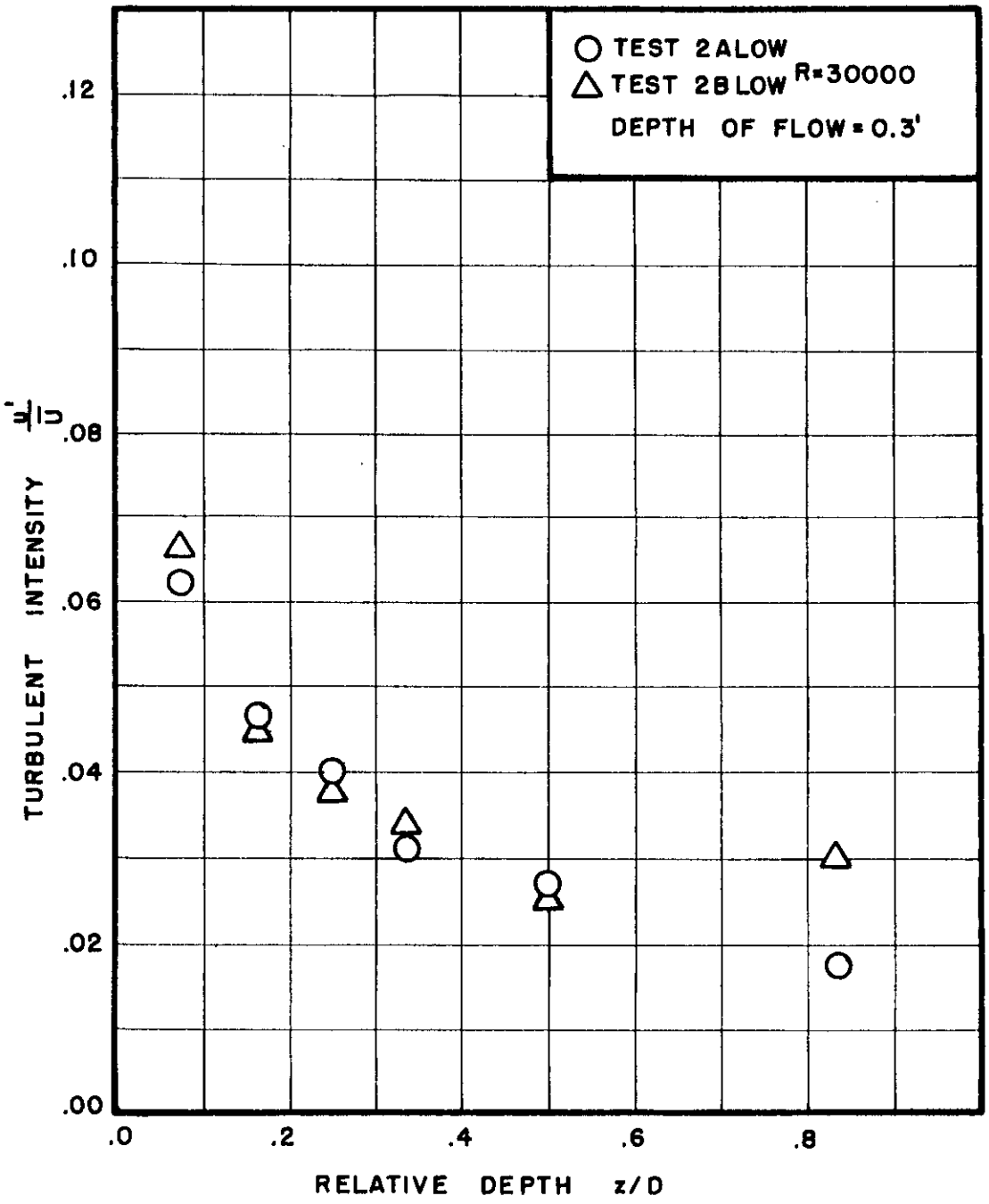

Figure 26. Turbulent Intensity Profiles for Tests 2A Low and 2B Low

cause the measurements to be in error; however, the error due to instrumentation accuracy would not account for the magnitude of the difference. It should be pointed out that these comparisons presume that the turbulent intensity is the same for a given Reynolds number. This has never been verified.

No data were taken on the effects of bed roughness on turbulent intensities. However, Figure 27 shows a comparison between Test 1A High and data from Rao's dissertation considering roughness as a parameter. Roughness increased the turbulent intensity near the bed, but had a small effect near the surface. The relative intensities reported by Rao are over five times larger near the bed than those in Test 1A High, but approximately two times greater for points near the water surface. Since the sediment concentration predictions made in this study used values of RMS velocity from the smooth channel, the magnitude of the diffusion coefficient for the rough sediment laden channel (which is proportional to the square of the RMS velocity) could be 25 times greater than that observed at the bed and four times greater than that observed at the water

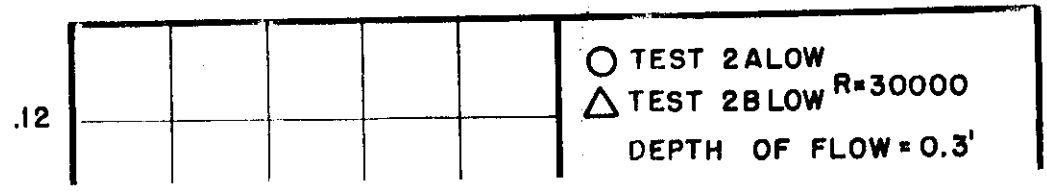

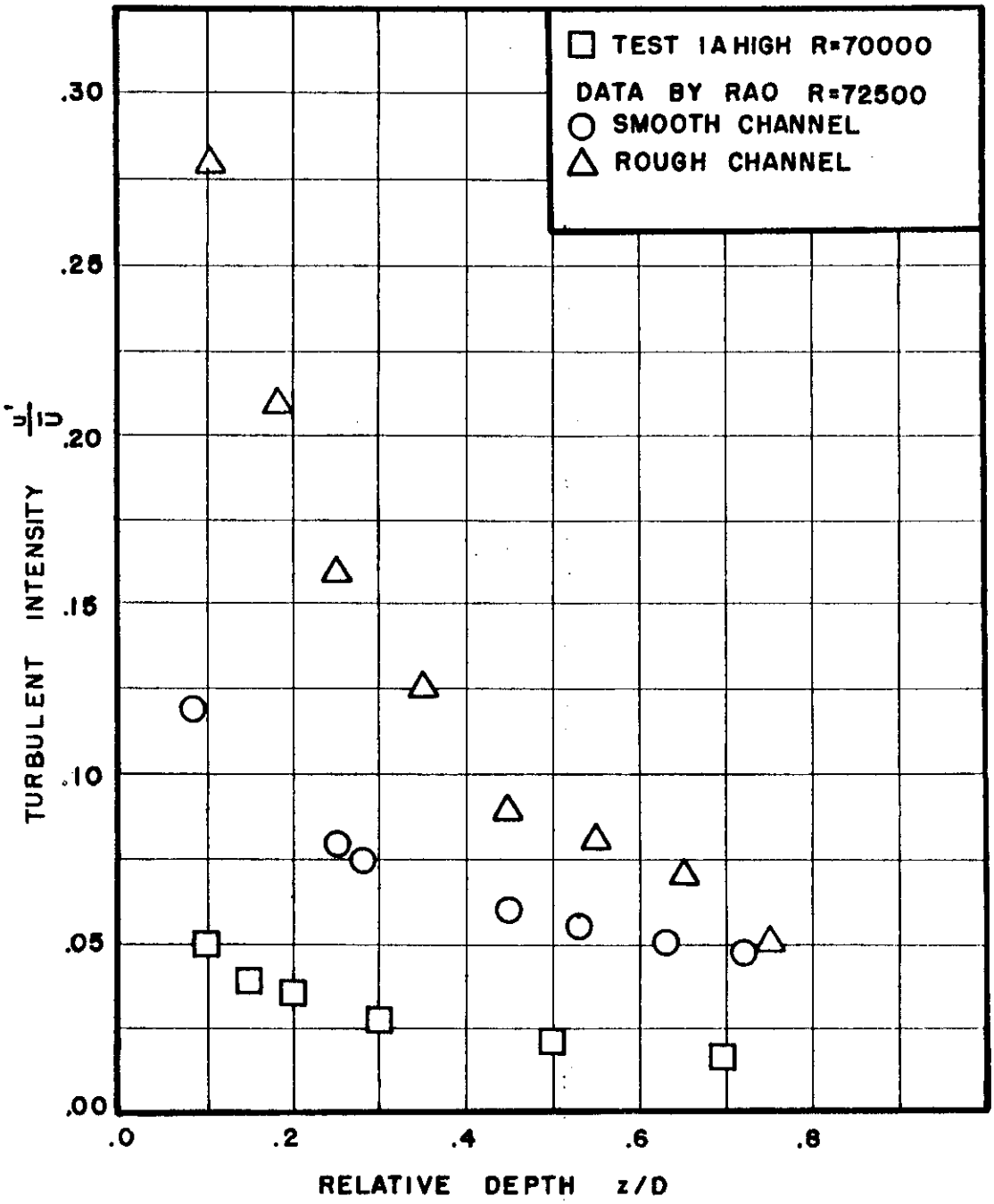

Figure 27. Comparison Between Turbulent Intensities for Test 1A High and Data Obtained by Rao

varies with depth, the diffusion coefficient will be a function of depth. Stated mathematically,

$$H(z) = u'^2(z)L_T(z)$$

where $H(z)$ is the diffusion coefficient. In an attempt to find the form of the functional relationship, linear regression, semi-logarithmic regression, and logarithmic linear regression were tried. A semi-logarithmic plot appeared to give the best representation. Figures 28 through 31 show plots of the diffusion coefficient versus depth and the resulting equation for H(z). In this form the diffusion coefficient as a function of depth can be represented in the exponential form $B'e^{A'z}$.

In each condition studied, the values for the diffusion coefficient near a relative depth of 0.1 were erratic. When plotted on logarithmic paper, a linear plot could be fit above a relative depth of approximately 0.1, but below 0.1 the curve had no well defined form. These considerations are based on a limited number of data points and are speculative in nature; however, further study of the diffusion coefficient at low relative depths could possibly yield a key to entrainment of sediment.

It should be noted at this point that the diffusion coefficient reported herein, which appears to monotomically decrease with depth, is different from that reported by Vanoni in his classic paper on sediment transportation (21). His relationship was a quadratic of the form $H(z) = a_1 z + a_2 z^2$. Since Vanoni's diffusion coefficient

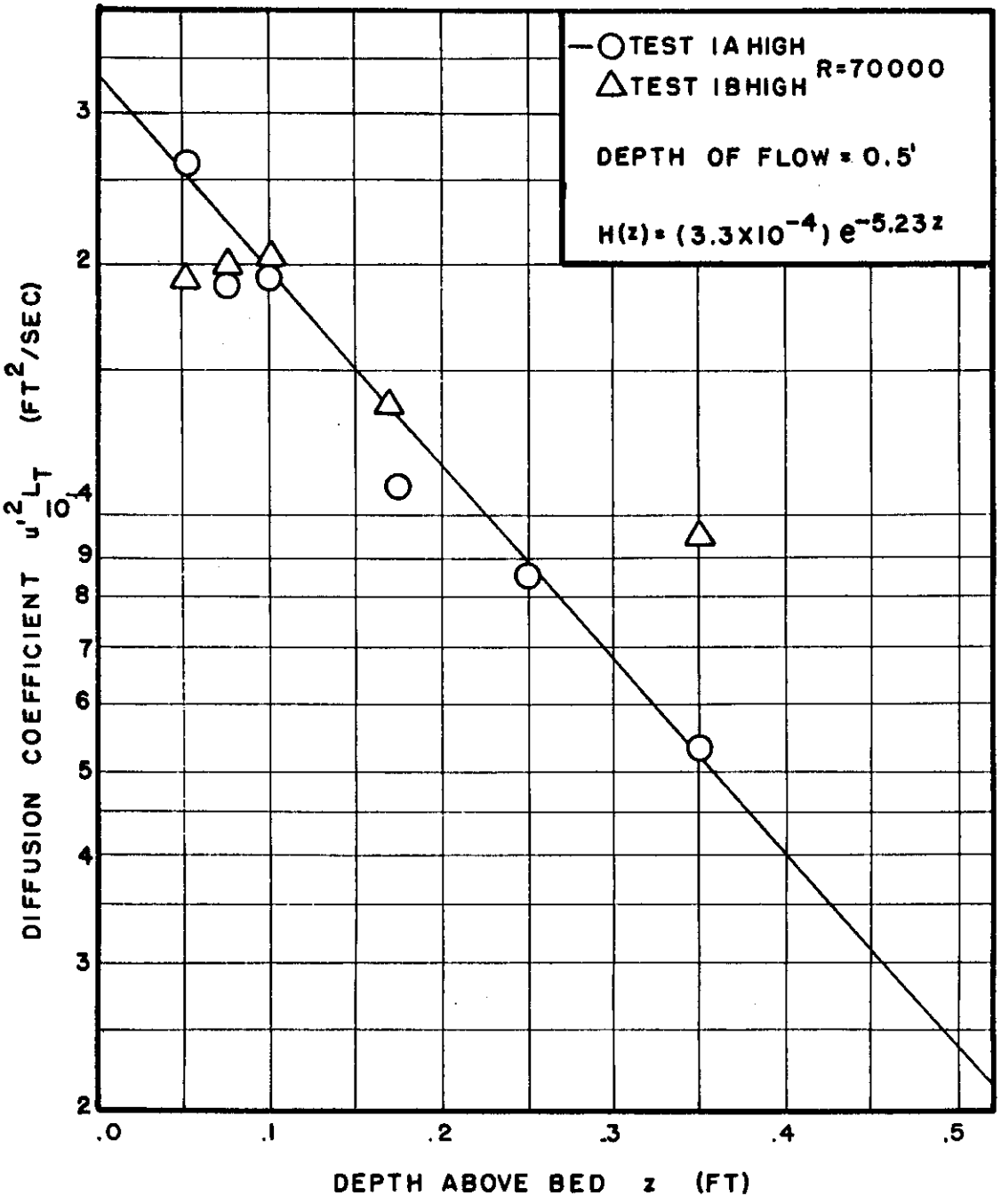

Figure 28. Diffusion Coefficient Profiles for Tests 1A High and 1B High

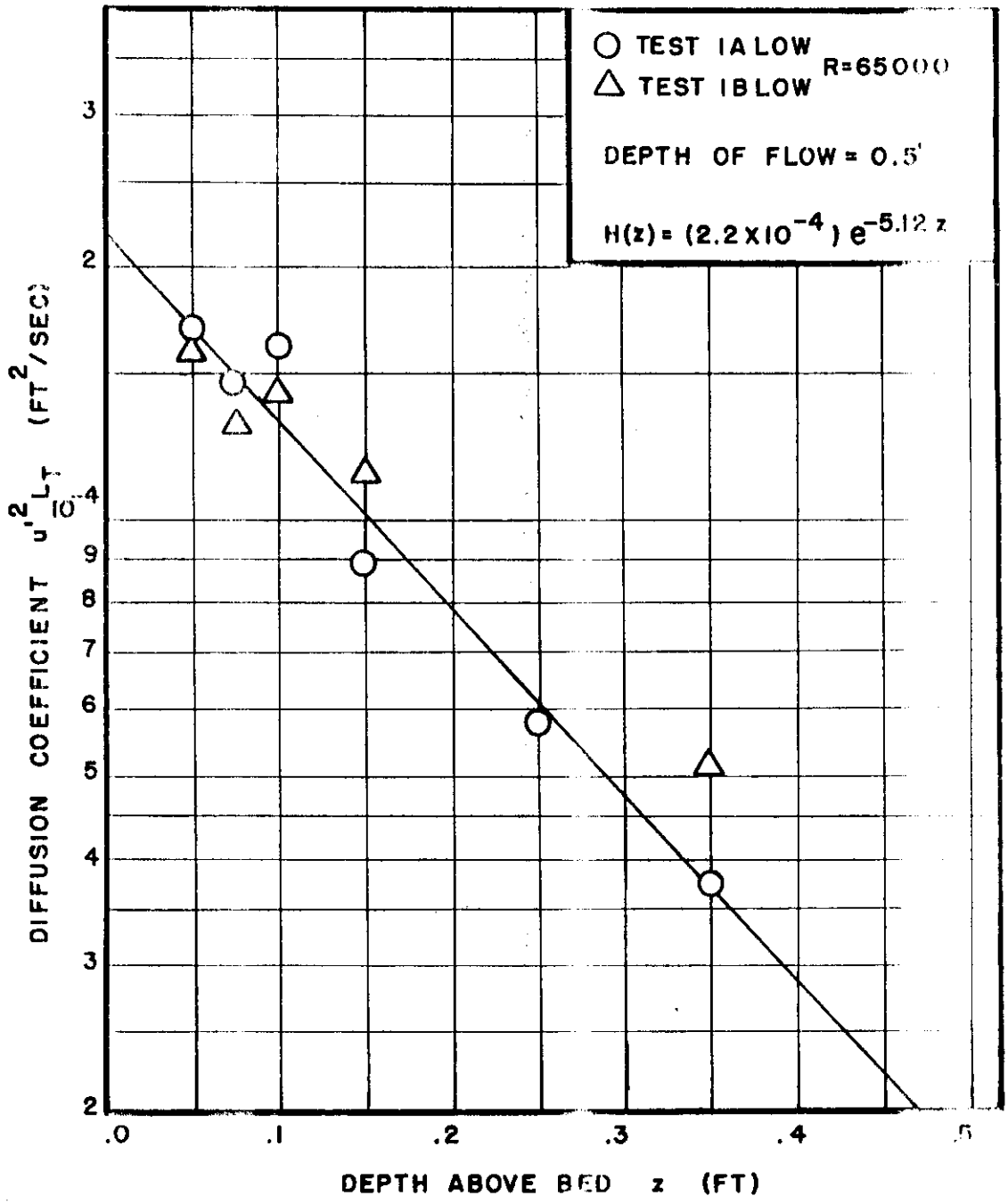

Figure 29. Diffusion Coefficient Profiles for Tests 1A Low and 1B Low

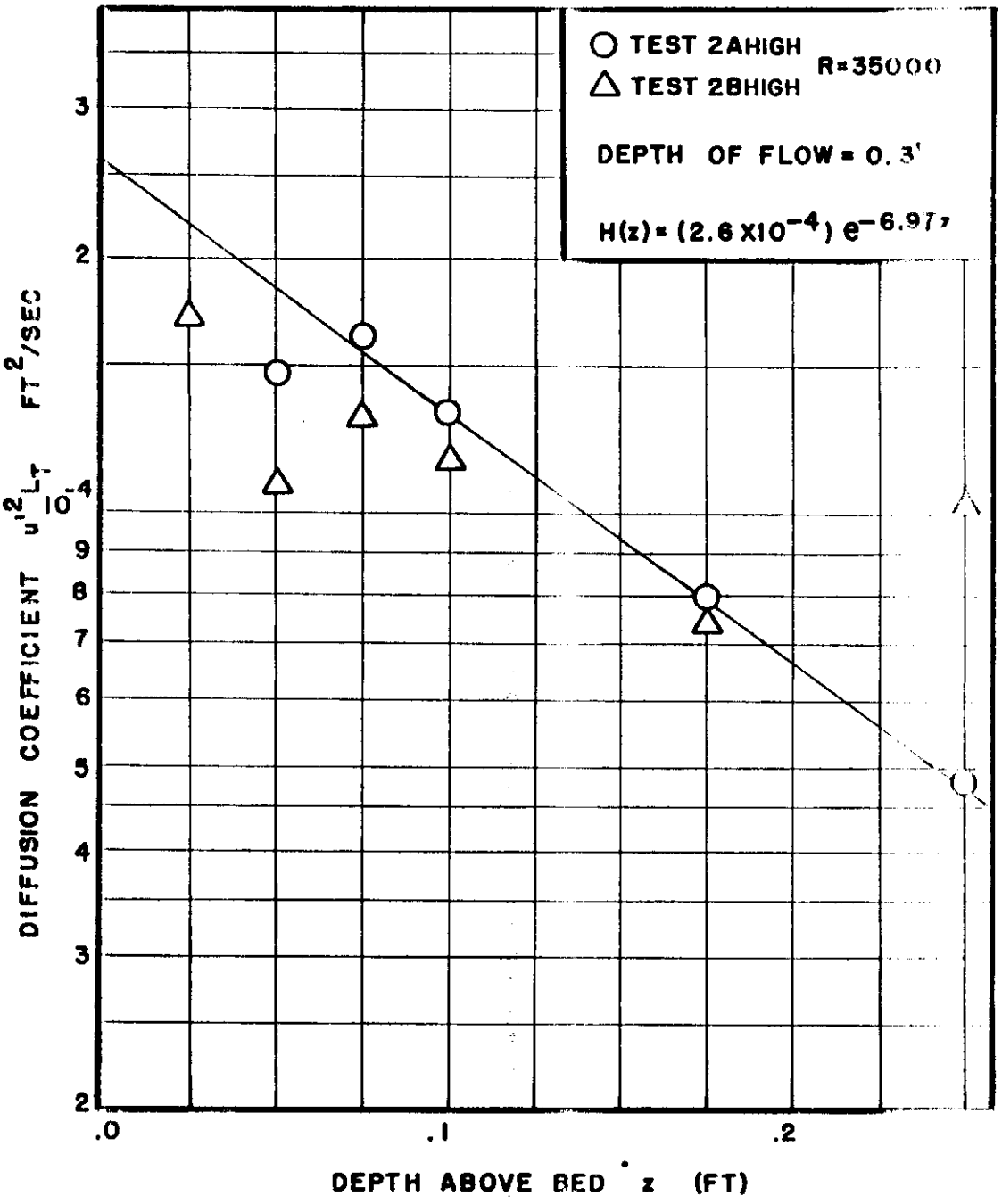

Figure 30. Diffusion Coefficient Profiles for Tests 2A High and 2B High

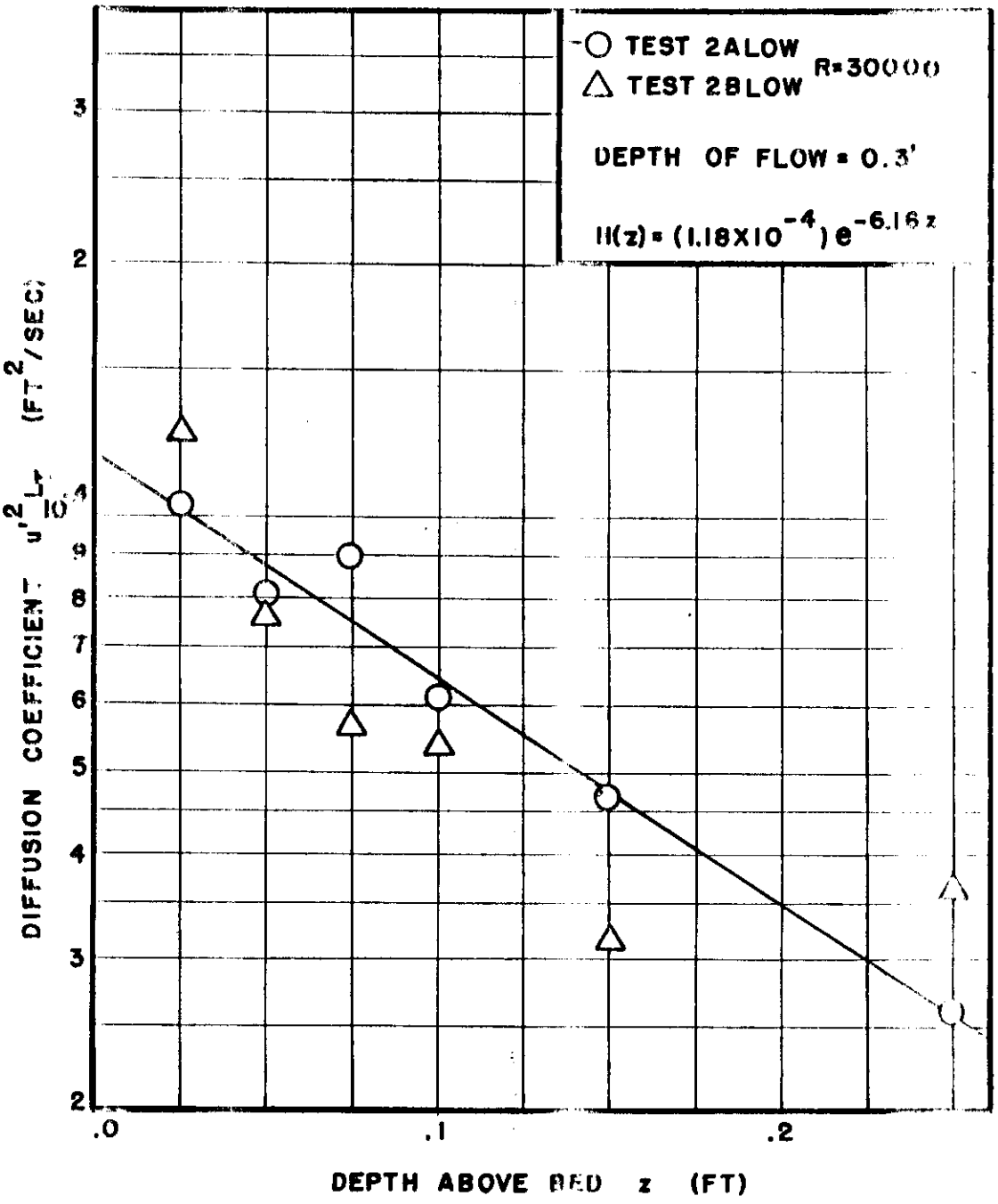

Figure 31. Diffusion Coefficient Profiles for Tests 2A Low and 2B Low

was determined by using the logarithmic velocity profile, as derived from mixing length theories, it is possible that the mixing length theory is in error.

In order to adequately describe the diffusion coefficient as a function of depth, more extensive measurements are needed than could be taken in this research with procedures available.

The Effects of Superimposed Rainfall on the Structure of Turbulence

One of the most significant results of the research conducted was the observation of the apparent effects of superimposed rainfall on the energy balance of turbulence in free surface flow. The correlograms shown earlier in Figures 19 through 23 show only a slight variation between rainfall and no rainfall for the test series 1 High and 1 Low (depth of flow = 0.5 ft.); however, for the test series 2 High and 2 Low (depth = 0.3 ft.) the difference in the correlograms near the free water surface is striking. For Tests 2 High and 2 Low, the time for which the autocorrelations becomes zero is markedly reduced by rainfall as previously shown in Figures 21 and 22. This was further evidenced in Figures 17 and 18 as a reduction in the time scale of turbulence. Since the spectral density function is the Fourier transform of the autocorrelation function, the result of decreasing the time for which correlation approaches zero is the same as increasing the energy spectrum at the higher frequencies. The high frequencies are the frequencies at which the turbulent energy is dissipated; therefore, it seems reasonable

that the net effect of rainfall at the lower depths of flow is to increase the viscous dissipation.

The effect of rainfall on the diffusion coefficient is somewhat difficult to ascertain since the data shown for rainfall test in Figures 28 through 31 exhibit a large amount of scatter. From a qualitative analysis of the profiles with rainfall it appears that the diffusion coefficient decreased slightly at the lower depths and increased at points near the water surface. This essentially made the diffusion coefficient more uniform with depth. A more uniform diffusion coefficient would in turn make the sediment concentration profile more uniform. The exact effect of rainfall on the concentration is difficult to determine experimentally due to the dilution effect caused by adding water of zero concentration at the free surface. Because of this dilution, no attempts were made to predict concentration profiles with superimposed rainfall.

Prediction of Sediment Profiles from Turbulence Data

Equation (53) was the final proposed non-steady state model for the prediction of sediment in two dimensional isotropic flow and is restated here for reference purposes.

$$\frac{\partial c}{\partial t} = u'^2 L_T \left[\frac{\partial^2 c}{\partial y^2} + \frac{\partial^2 c}{\partial x^2} \right] + \underline{K} \frac{\partial c}{\partial z} \quad . \tag{53}$$

For the case of interest in this research, the slope of the gradient in the direction of flow (y coordinate) is much less than in the

vertical direction (z coordinate), or,

$$\frac{\partial^2 c}{\partial y^2} << \frac{\partial^2 c}{\partial z^2} \quad .$$

Therefore, equation (53) can be written as

$$\frac{\partial c}{\partial t} = u'^2 L_T \frac{\partial^2 c}{\partial z^2} + \underline{K} \frac{\partial c}{\partial z} \quad . \tag{54}$$

Once a steady condition has been reached, $\frac{\partial c}{\partial t}$ becomes zero and equation (53) can be written as

$$u'^2 L_T \frac{d^2 c}{dz^2} + \underline{K} \frac{dc}{dz} = 0 \quad . \tag{55}$$

In the tests run, it was assumed that steady state conditions had been reached at the instrument section. Using the exponential form of the diffusion coefficient suggested earlier, equation (55) becomes

$$B' e^{A'z} \frac{d^2 c}{dz^2} + \underline{K} \frac{dc}{dz} = 0 \quad . \tag{56}$$

Equation (56) can be written alternately as

$$\frac{dc}{dz} = C_1 \exp \left[\frac{\underline{K}}{A'B'} e^{-A'z} \right] \tag{57}$$

which has the solution

$$c = C_1 \int_0^z \exp \left(\frac{\underline{K}}{A'B'} e^{-A'z'} \right) dZ' + C_2 \tag{58}$$

in which C_1 and C_2 are constants of integration. Since equation (58) has no known analytical solution, it was solved by numerical integration using a depth interval of 0.0001 ft. and double precision arithmetic on an IBM 7094 computer.

The upper boundary was treated as a reflecting wall which means that the flux crossing it becomes zero. This is expressed mathematically (see Chandrasekhar) as

$$B'e^{A'z}\frac{dc}{dz}\left|_{(z = D_f)^{\pm Kc}}\right| z = D_f = 0 \quad . \tag{59}$$

The other boundary condition chosen was the concentration measured at a depth of 0.05 ft., or

$$c(.05) = C_1 \int_0^{.05} \exp\left[\frac{K}{A'B'} e^{-A'z}\right] dz' + C_2 \quad . \tag{60}$$

The lower boundary is a partially absorbing barrier which is difficult to express mathematically. For this reason, the boundary condition expressed by equation (60) was selected. Table 3 shows the constants used and the resulting differential equation in each test.

Comparison of Predicted Versus Observed Concentrations. The predicted and observed concentrations are plotted in Figures 32 through 35. The predicted concentration profile based on the values of B' and A' determined in this research are shown by the solid lines. In every case the values predicted by the differential equation are negligible compared to the observed values. This leaves two plausible conclusions: that the measured turbulence input parameters were wrong, or that the mathematical model is invalid.

Possible Sources of Error in Input Turbulence Parameters. As mentioned previously, the turbulence measurements were made in

TABLE 3

EQUATIONS USED FOR COMPUTER SOLUTION

Test 1A High $A' = -5.23, \quad B' = 3.3 \times 10^{-4}, \quad \underline{K} = .0080$

$$(3.3 \times 10^{-4}\, e^{-5.23z}) \frac{d^2c}{dz^2} + .0080 \frac{dc}{dz} = 0$$

Test 1A Low $A' = -5.12, \quad B' = 2.2 \times 10^{-4}, \quad \underline{K} = .0131^*$

$$(2.2 \times 10^{-4}\, e^{-5.12z}) \frac{d^2c}{dz^2} + .0131 \frac{dc}{dz} = 0$$

Test 2A High $A' = -6.97, \quad B' = 2.6 \times 10^{-4}, \quad \underline{K} = .0040$

$$(2.6 \times 10^{-4}\, e^{-6.97z}) \frac{d^2c}{dz^2} + .0040 \frac{dc}{dz} = 0$$

Test 2A Low $A' = -6.16, \quad B' = 1.18 \times 10^{-4}, \quad \underline{K} = .0038^*$

$$(1.18 \times 10^{-4}\, e^{-6.16z}) \frac{d^2c}{dz^2} + .0038 \frac{dc}{dz} = 0$$

*The variation in $\underline{K}$ between Test 1A High and 1A Low and between 2A High and 2B Low is due to a difference in water temperature.

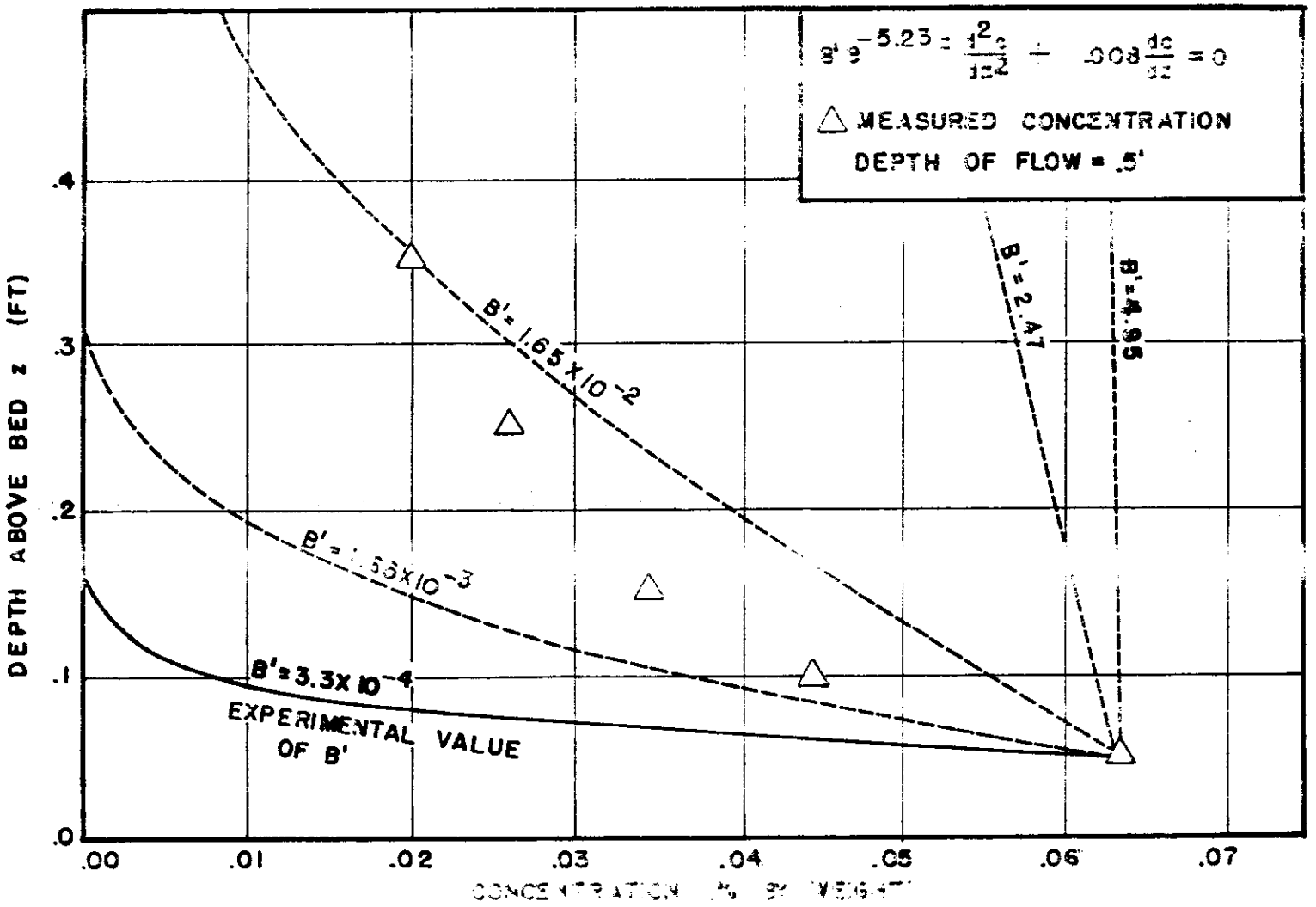

Figure 32. Predicted Concentrations for Test 11 High

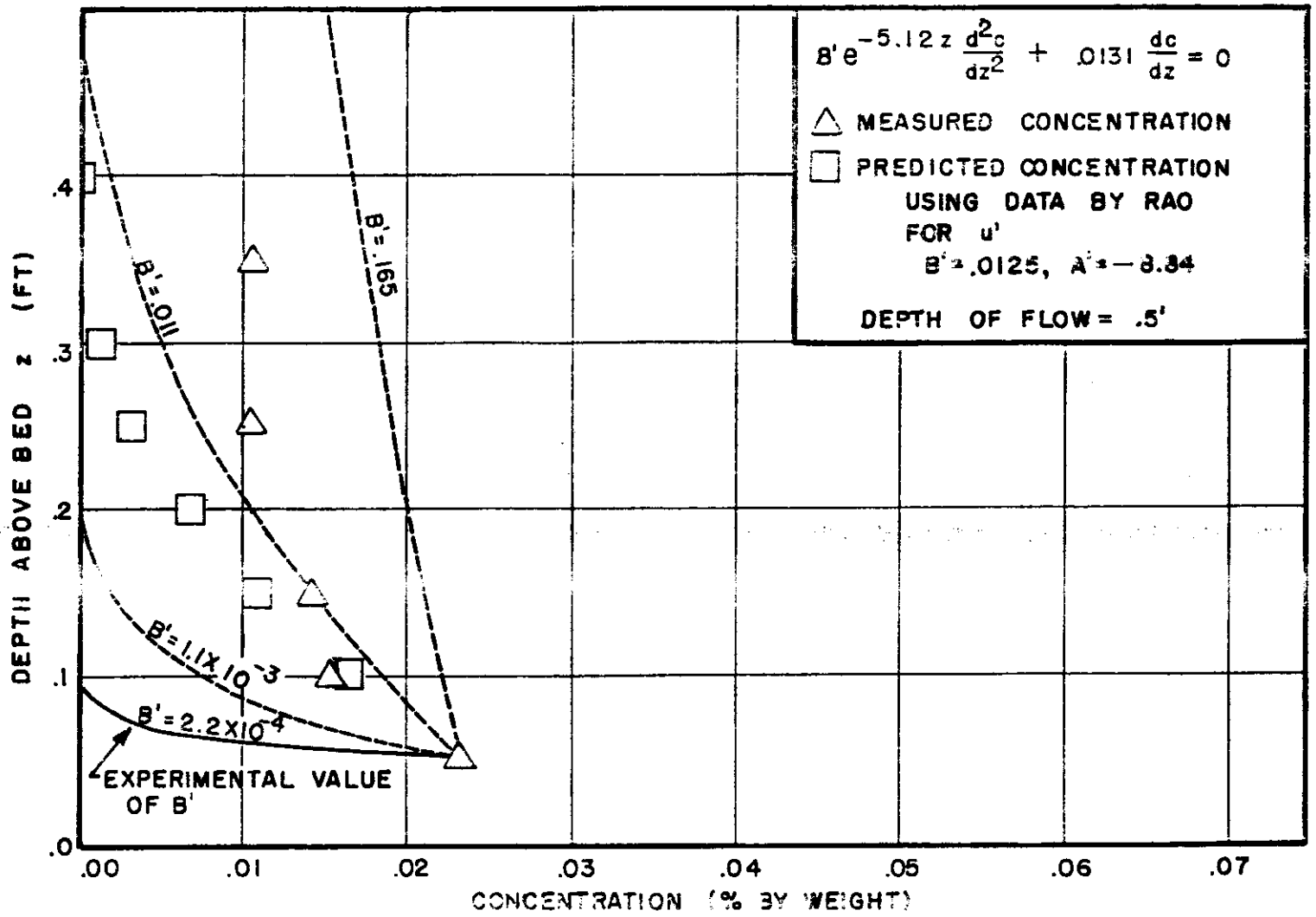

Figure 33. Predicted Concentrations for Test 1A Low

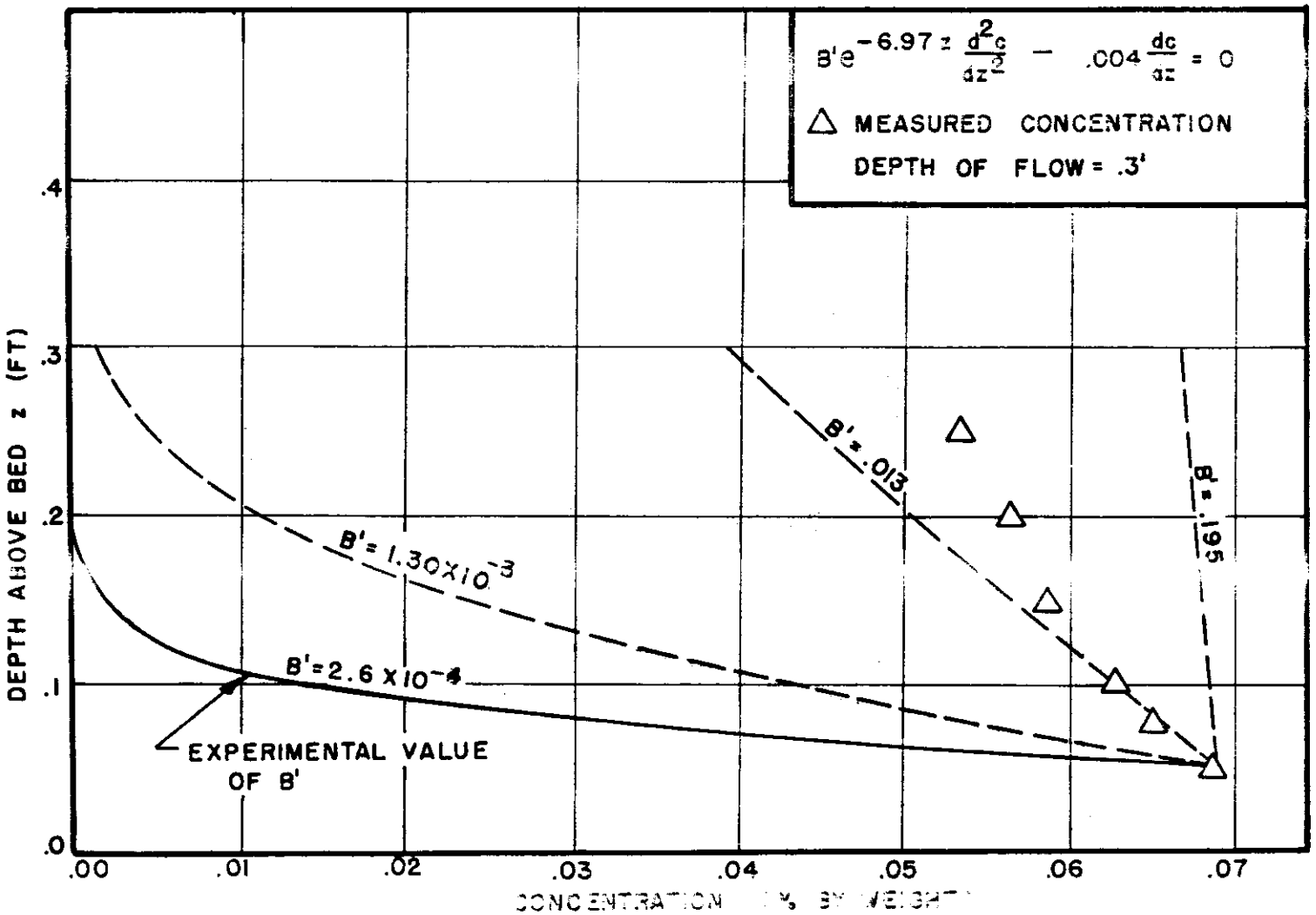

Figure 3-1. Predicted Concentrations for Test 2A High

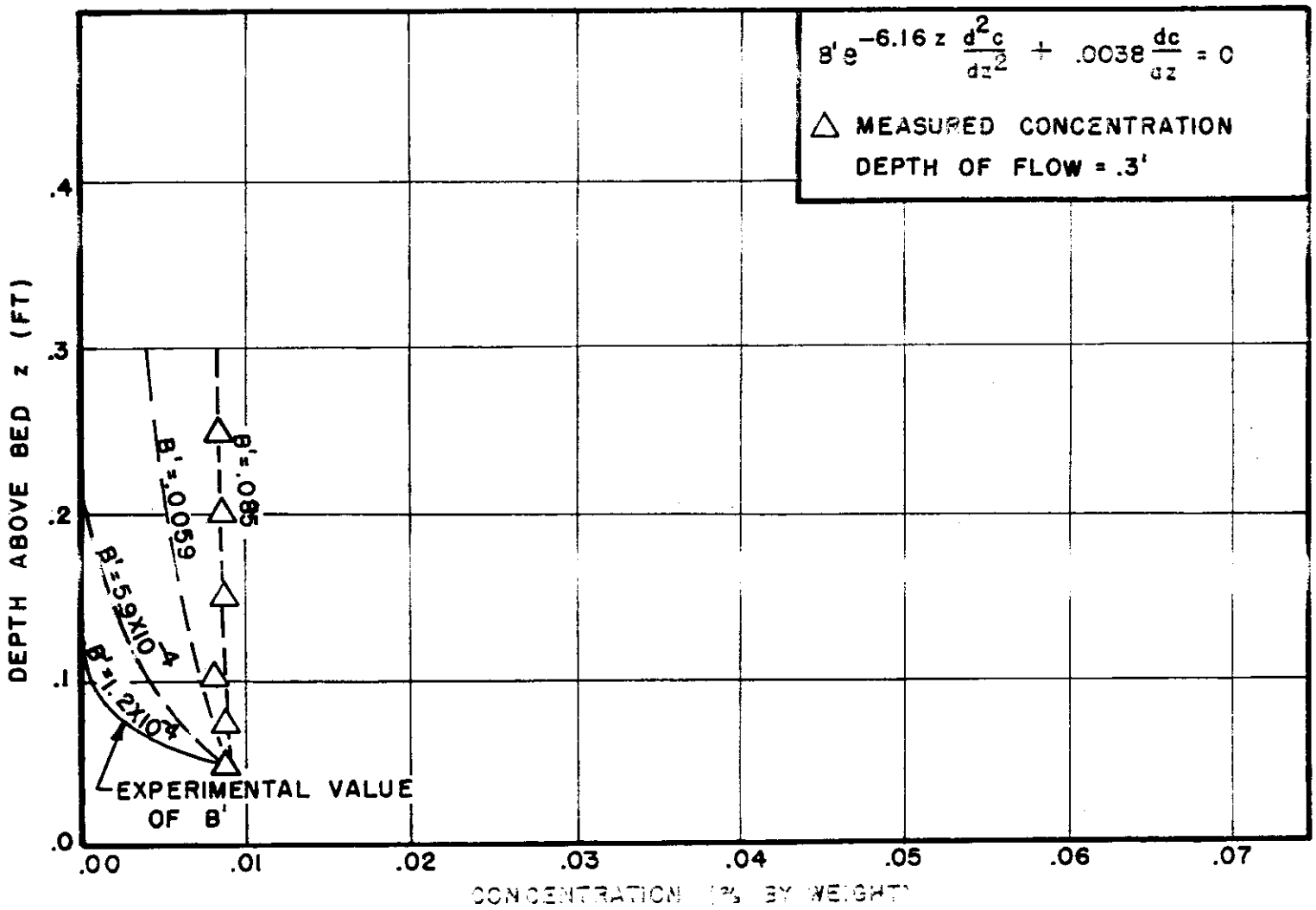

Figure 35. Predicted Concentrations for Test 2A [illegible]

sediment free water with a smooth bed, whereas the sediment laden water had a rough bed as shown by Figure 36. Also, the turbulent intensity for the rough bed was shown to be much greater than for the smooth bed. Due to this large difference between the rough and smooth case, the value of B' in the equation for the diffusion coefficient was varied to ascertain the effect on the predicted concentration profiles. These profiles are shown in Figures 32 through 35 by the dashed lines. Since the diffusion coefficient is proportional to the RMS velocity, an increase in the RMS velocity will result in an increase in B'. It should be noted that A' will also change as the RMS velocity is varied, but this variation was not studied due to the large amount of computer time involved. As can be seen by predicted concentration profiles previously shown in Figures 32 to 35, increasing B' by a factor of approximately 15 yielded concentrations in the same range as those observed in this research. Rao's data indicated that the turbulent intensities for the roughened bed are from three to five times those of the smooth bed as was shown in Figure 27; hence, it is probable that the measured values of turbulence for the smooth bed are too low for the case of a bed covered with sediment. A predicted concentration profile is shown in Figure 33 for the flow conditions of Test 1A High using turbulent intensities for a rough bed obtained from Rao. This profile is not intended to be an absolute prediction but a qualitative analysis of the effects of bed roughness on the diffusion of sediment.

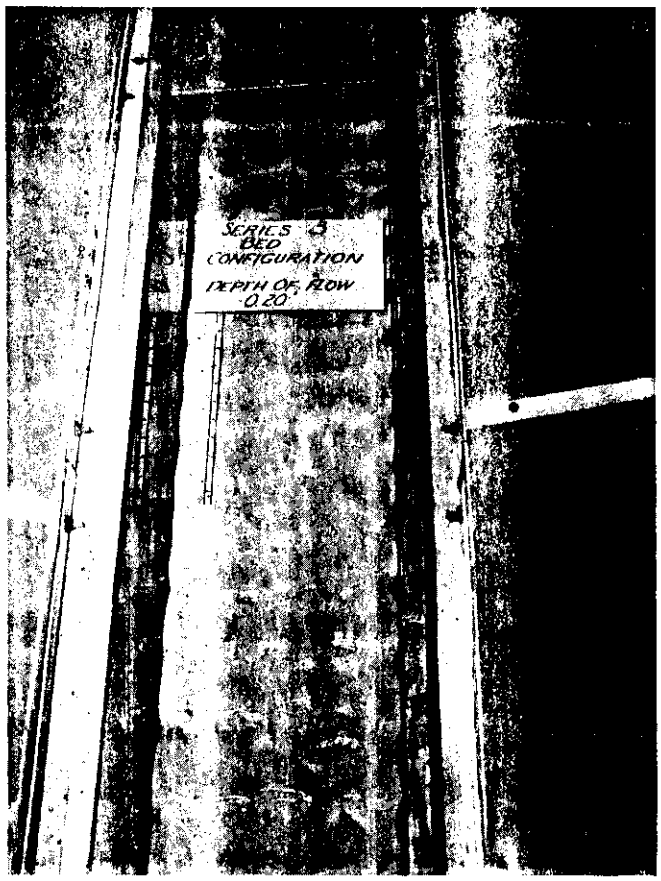

Figure 36. Photograph of Flume Bed Showing Dune Formations

The equation predicted much higher concentrations using Rao's data which indicates the sensitivity of the mathematical model to RMS velocities.

A comparison of the magnitude of the diffusion coefficient with that of Hiler et al. in water at near laminar flow (Reynolds number $\simeq$ 60) further leads one to believe that the RMS velocity values used in the equation were too low (8). In the Hiler et al. data, the diffusion coefficient was 2.0×10^{-2} cm.^{2}/sec. or approximately 2.0×10^{-5} ft.^{2}/sec. As shown earlier in Figures 28 through 31, the values for the diffusion coefficient in this study ranged from approximately 2.0×10^{-5} ft.^{2}/sec. to 3.0×10^{-5} ft.^{2}/sec.

Based on these comparisons to the Hiler et al. data and Rao's data, it is probable that the RMS velocities used in the equation were too low. Further measurements need to be made in flow with sediment laden water in order to either reject or accept the mathematical model.

Possible Errors in the Mathematical Model. The weakest point in the derivation of the model given by equation (53) concerns the structure of β, the drag coefficient. The basic derivation assumes that a discrete fluid particle maintains its identity and that the turbulence is constant in time and space when in reality it is not. The verse quoted in many circles of fluid mechanicians proves the point somewhat facetiously:

"Big eddies have little eddies
And feed on their velocities.
Little eddies have smaller eddies,
And so on to viscosity." Q.E.D

In the derivation of the mathematical model, it was assumed that a drag coefficient could be identified with a fluid particle. In the final use of the derived equation, however, a value for β determined for a sediment particle was used. The effect of this substitution has not been determined. The Hiler et al. verification of the basic equation for flow with an electric force field lends some credence to the use of the value of β determined from the sediment particle, although his flow conditions were quite different.

CHAPTER VI

SUMMARY AND CONCLUSIONS

The structure of turbulence in streams affects the suspended sediment carrying capability. Due to the random nature of turbulence, sediment movement can be analyzed as a stochastic process. Starting with the Langevin equation modified for a turbulent medium, a partial differential equation was developed which describes the change in sediment concentration with time and space in two dimensional open channel flow with isotropic turbulence. The input parameters to the equation were the fall velocity of the sediment particles and the turbulent diffusion coefficient. The diffusion coefficient used was the product of the mean square velocity and the Eulerian time scale of turbulence.

A 40 ft. recirculating research flume was used for the experimental investigations. The RMS velocity and Eulerian time scale profiles were determined by the use of a hot-film anemometer and a random signal correlator. The effect of rainfall on the RMS velocities and time scales was observed. Sediment concentration profiles were measured by withdrawing samples from the flow and were compared with the values predicted by the partial differential equation.

The following conclusions were made from this study:

1. The Eulerian time scale is relatively constant with depth. In all of the observed profiles, no trend with depth

could be detected.

2. Rainfall on a free water surface tends to decrease the time scale of turbulence. This is most evident in shallow flows where the energy input of the rainfall has a large effect on the total energy of the system. The decrease in time scale will result in an increase in viscous dissipation of energy.

3. The diffusion coefficient is a decreasing function of depth. An exponential function appears to best describe the relationship between diffusion and depth with the exception of points near the channel bed where a large amount of variation was observed.

4. Turbulent diffusion is highly sensitive to RMS fluid velocities. Since the diffusion coefficient is proportional to the square of the RMS velocity, a variation in the RMS velocity is magnified in the equation for diffusion.

As a result of this investigation, the following areas are recommended for future study:

1. The optimum sampling time for measuring representative correlograms should be investigated. Since the use of the correlograms assumes that the time average is the statistical average, a study of the times required for an accurate estimate of the correlogram of turbulent velocity fluctuations is needed. A report on the variability of correlograms with differing sample times would also be valuable in planning future research.

2. Knowledge of the variation in RMS velocities between a smooth bed and a rough moveable bed would be useful in an analysis of the effects of a rough bed on turbulent diffusion and on the energy balance of a system. Past studies have been conducted on a fixed bed or an artificially roughened stationary bed. An alluvial bed does not fit either category.

3. The structure of the diffusion coefficient at low relative depths warrants further study since it is closely tied to entrainment of sediment from the bed.

4. An investigation of the possibility of describing the diffusion coefficient as a function of flow conditions should be undertaken. This information would eliminate the necessity of measuring the turbulence characteristics of a channel before attempting to predict the sediment carrying capability.

5. The structure of the viscous drag coefficient for turbulent flow conditions should be investigated. Included in this study should be an investigation of the effects of turbulence on the fall velocity of a particle. In the alternate derivation of the theoretical model given in Chapter III, a Gaussian distribution of particle displacements with a non-zero mean equal to the product of the mean fall velocity and time was assumed. The value of the mean fall velocity was determined using Stokes law for a still medium; however, it is probable that the mean fall velocity is dependent on turbulent intensity.

APPENDIX A

SOME THEORETICAL RELATIONSHIPS

USED IN

FORMULATING THE MATHEMATICAL MODEL

1. The Space Derivatives of Probability Density Functions

Based on the inversion theorem of the characteristic function, the following steps are self explanatory.

$$P[\underline{x}(t)] = \frac{1}{8\Pi^3}\iiint \Phi(\underline{\xi},t)e^{-i\underline{\xi}\ \underline{x}}\, d\underline{\xi} \qquad (a)$$

$$\frac{\partial P[\underline{x}(t)]}{\partial x_j} = i\xi_j \iiint \Phi(\underline{\xi},t)e^{-i\ \underline{\xi}\ \underline{x}}\, d\underline{\xi} \qquad (b)$$

$$\frac{\partial^2 P[\underline{x}(t)]}{\partial x_i\, \partial x_j} = i^2\xi_i\xi_j \iiint \Phi(\underline{\xi},t)e^{-i\ \underline{\xi}\ \underline{x}}\, d\underline{\xi} \qquad (c)$$

$$\frac{\partial^2 P[\underline{x}(t)]}{\partial x_i\, \partial x_j} = -\xi_i\xi_j\, P[\underline{x}(t)] \qquad (d)$$

11. The Time Derivative of the Mean Square Dispersion

The following steps are based on convergence of the derivative in the mean square sense and are taken essentially from Batchelor (1). Let $X_i(t)$ be the ith component of displacement of a fluid particle at time t. Then

$$\overline{\left[\frac{d[X_i(t)X_j(t)]}{dt}\right]} = \overline{\left[X_j(t)\ \frac{d}{dt}[X_i(t)] + X_i(t)\ \frac{d}{dt}[X_j(t)]\right]} \qquad (e)$$

$$= \overline{X_j(t)\ v_i(t) + X_i(t)\ v_j(t)} \quad . \qquad (f)$$

However,

$$X_i(t) = \int_0^t v_i(\tau)\, d\tau \quad . \tag{g}$$

It follows, therefore, that

$$\left[\overline{\frac{d[X_i(t)\ X_j(t)]}{dt}}\right] = \int_0^t \overline{v_i(\tau)\ v_j(\tau)}\ d\tau + \int_0^t \overline{v_i(\tau) v_j(\tau)}\ d\tau \quad . \tag{h}$$

The following expressions follow from the definition of a derivative.

$$\overline{\frac{d}{dt}[X_i(t)\ X_j(t)]} = \overline{\lim_{h\to o} \frac{X_i(t+h)\ X_j(t+h) - X_i(t)X_j(t)}{h}} \tag{i}$$

$$= \lim_{h\to o} \frac{\overline{X_i(t+h)\ X_j(t+h) - X_i(t)X_j(t)}}{h} \tag{j}$$

$$= \frac{d}{dt}\overline{[X_i(t)\ X_j(t)]} \quad . \tag{l}$$

Using equation (k) and equation (h) and assuming that $\underline{X}(t)$ is a covariant stationary process, then

$$\frac{d}{dt}\overline{[X_i(t)\ X_j(t)]} = v_i' v_j' \int_0^t \left[R_{ij}(\tau)\ d\tau + R_{ji}(\tau)\ d\tau\right] \tag{l}$$

in which

$$R(\varepsilon) = \frac{\overline{v_i(t)\, v_j(\tau)}}{v_i' v_j'}$$

and $\varepsilon = \tau - t$.

111. Relationship Between the Spectral Density of the Fluid and the Particle Velocities

The relationships given below are an expansion of those outlines by Csanady (5). The deviation between the spectral density of the fluid velocity and the particle velocity is due to the fact that the heavy particles react to accelerative forces more slowly than a fluid medium resulting in relative motion between a particle and its surrounding medium. This relative motion can be expressed as

$$\frac{dv_p}{dt} = \beta(v_p - v_f) \quad . \tag{m}$$

The particle and fluid velocities can be expressed in terms of a stochastic Fourier-Stieltjes Integral as

$$v_p = \int e^{i\omega t}\, dZ_p(\omega) \tag{n}$$

and

$$v_f = \int e^{-i\omega t}\, dZ_f(\omega) \tag{o}$$

in which $Z(\omega)$ is a process with orthogonal increments. Using equations (n) and (o), equation (m) becomes

$$\frac{dv_p}{dt} = i\omega \int e^{i\omega t}\, dZ_p(\omega) \tag{p}$$

Equation (p) can be written as

$$[i\omega + \beta] \int e^{i\omega t}\, dZ(\omega) = \beta \int e^{i\omega t}\, dZ_p(\omega) \quad . \tag{q}$$

Hence

$$v_p = \int \frac{e^{i\omega t}}{i\omega + \beta}\, dZ_f(\omega) \quad . \tag{r}$$

The spectra is obtained by multiplying by the complex conjugate, or

$$\overline{v_p^2} = \overline{\int \frac{\beta}{i\omega + \beta}\, e^{i\omega t}\, dZ_f(\omega) \int \frac{\beta}{-i\omega + \beta}\, e^{-i\omega t}\, dZ_f^*(\omega)}$$

$$= \int \frac{\beta^2}{\beta^2 + \omega^2}\, \overline{dZ_f(\omega)\, dZ_f^*(\omega)} \quad . \tag{s}$$

However, $Z_f(\omega)$ has the properties due to orthogonal increments that

$$\overline{dZ_f(\omega)\, dZ_f^*(\omega)} = \Phi_f(\omega) d\omega \qquad \text{if } Z_f = Z_f^*$$

$$= 0 \qquad \text{if } Z_f \neq Z_f^* \ .$$

Therefore, it follows that

$$\overline{v_p^2} = \int \frac{\beta^2}{\beta^2 + \omega^2}\, \Phi_f(\omega) d\omega \ . \tag{t}$$

APPENDIX B

SUMMARY OF DATA

TABLE 4

SUMMARY OF DATA
DEPTH OF FLOW = 0.5 FT.

TEST 1A HIGH
NO RAINFALL

Depth Above Bed z Ft.	Mean Velocity U_m Ft./Sec.	Reynolds Number R ---	RMS Velocity u' Ft./Sec.	Turbulent Intensity $\frac{u'}{\overline{U}}$	Eulerian Length Scale L_T Sec.	Diffusion Coefficient $u'^2 L_T$ $Ft.^2/Sec.$	Sediment Concentration c %	Sediment Diameter d in.
.40	1.45	70,000	---	---	.1396	---	---	.0020
.35			.0192	.0173	.1444	5.32×10^{-5}	.0200	
.30			---	---	.1447	---	---	
.25			.6233	.0213	.1566	8.50×10^{-5}	.0260	
.20			---	---	.1417	---	---	
.175			.0287	.0277	.1305	1.07×10^{-4}	---	
.150			---	---	.1592	---	.0344	
.125			---	---	.1303	---	---	
.100			.0368	.0376	.1418	1.92×10^{-4}	.0447	
.075			.0373	.0399	.1358	1.89×10^{-4}	---	
.050			.0447	.0496	.1313	2.62×10^{-4}	.0622	
.033			---	---	---	---	.3713	

TABLE 5

SUMMARY OF DATA
DEPTH OF FLOW = 0.5 FT.

TEST 1B HIGH
RAINFALL

Depth Above Bed z	Mean Velocity U_m	Reynolds Number R	RMS Velocity u'	Turbulent Intensity $\frac{u'}{\bar{U}}$	Eulerian Length Scale L_T	Diffusion Coefficient $u'^2 L_T$	Sediment Concentration c	Sediment Diameter d
Ft.	Ft./Sec.	---	Ft./Sec.		Sec.	$Ft.^2/Sec.$	%	in.
.40	*	*	---	---	.107	---	---	.0020
.35			.0246	.0210	.152	9.18×10^{-5}	.0179	
.30			---	---	.112	---	---	
.25			.0267	.0233	---	---	.0207	
.20			---	---	.113	---	---	
.175			---	---	---	---	---	
.150			.0305	.0285	.145	1.35×10^{-4}	.0268	
.125			---	---	---	---	---	
.100			.0347	.0344	.170	2.05×10^{-4}	.0282	
.075			.0366	.0389	.145	1.94×10^{-4}	---	
.050			.0414	.0486	.108	1.84×10^{-4}	.0404	
.025			---	---	.125	---	.3093	

*Approximately the same as test 1A High

TABLE 6

SUMMARY OF DATA
DEPTH OF FLOW = 0.5 FT.

TEST 1A LOW
NO RAINFALL

Depth Above Bed z Ft.	Mean Velocity U_m Ft./Sec.	Reynolds Number R ---	RMS Velocity u' Ft./Sec.	Turbulent Intensity $\frac{u'}{\bar{U}}$ ---	Eulerian Length Scale L_T Sec.	Diffusion Coefficient $u'^2 L_T$ $Ft.^2/Sec.$	Sediment Concentration c %	Sediment Diameter d in.
.40	1.34	65,000	---	---	.136	---	---	.0020
.35			.0167	.0166	.133	3.71×10^{-5}	.0109	
.30			---	---	.126	---	---	
.25			.0215	.0219	.125	5.78×10^{-5}	.0103	
.20			---	---	.160	---	---	
.175			---	---	.145	---	---	
.150			.0241	.0263	.154	8.93×10^{-5}	.0141	
.125			---	---	.171	---	---	
.100			.0310	.0357	.168	1.60×10^{-4}	.0153	
.075			.0325	.0396	.140	1.47×10^{-4}	---	
.050			.0356	.0456	.133	1.68×10^{-4}	.0231	
.025			---	---	---	---	.1246	

TABLE 7

SUMMARY OF DATA
DEPTH OF FLOW = 0.5 FT.

TEST 1B LOW
RAINFALL

Depth Above Bed z Ft.	Mean Velocity U_m Ft./Sec.	Reynolds Number R ---	RMS Velocity u' Ft./Sec.	Turbulent Intensity $\frac{u'}{\overline{U}}$	Eulerian Length Scale L_T Sec.	Diffusion Coefficient $u'^2 L_T$ $Ft.^2/Sec.$	Sediment Concentration c %	Sediment Diameter d in.
.40	*	*	---	---	.108	---	---	.0020
.35			.0209	.0204	.118	5.15×10^{-5}	.0096	
.30			---	---	.197	---	---	
.25			.0237	.0235	---	---	.0126	
.20			---	---	.131	---	---	
.175			---	---	---	---	---	
.150			.0284	.0297	.142	1.15×10^{-4}	.0147	
.125			---	---	---	---	---	
.100			.0315	.0344	.143	1.42×10^{-4}	.0170	
.075			.0324	.0376	.124	1.30×10^{-4}	---	
.050			.0357	.0450	.126	1.60×10^{-4}	.0202	
.025			---	---	.114	---	.1145	

*Approximately the same as test 1A Low

TABLE 8

SUMMARY OF DATA
DEPTH OF FLOW = 0.3 FT

TEST 2A HIGH
NO RAINFALL

Depth Above Bed z	Mean Velocity U_m	Reynolds Number R	RMS Velocity u'	Turbulent Intensity $\frac{u'}{\bar{U}}$	Eulerian Length Scale L_T	Diffusion Coefficient $u'^2 L_T$	Sediment Concentration c	Sediment Diameter d
Ft.	Ft./Sec.	---	Ft./Sec.		Sec.	$Ft.^2/Sec.$	%	in.
.250	1.13	35,000	.0201	.0199	.117	4.73×10^{-5}	.0535	.0011
.200			---	---	.119	---	.0565	
.175			---	---	.109	---	---	
.150			.0274	.0320	.105	7.92×10^{-5}	.0588	
.125			---		.101	---	---	
.100			.0328	.0417	.123	1.32×10^{-4}	.0628	
.075			.0357	.0479	.127	1.62×10^{-4}	.0652	
.050			.0374	.0533	.104	1.46×10^{-4}	.0659	
.025			.0446	.0701	---	---	.3847	

TABLE 9

SUMMARY OF DATA
DEPTH OF FLOW = 0.3 FT.

TEST 2B HIGH
RAINFALL

Depth Above Bed z Ft.	Mean Velocity U_m Ft./Sec.	Reynolds Number R ---	RMS Velocity u' Ft./Sec.	Turbulent Intensity $\frac{u'}{\overline{U}}$	Eulerian Length Scale L_T Sec.	Diffusion Coefficient $u'^2 L_T$ $Ft.^2/Sec.$	Sediment Concentration c %	Sediment Diameter d in.
.250	*	*	.0389	.0396	.066	1.00×10^{-4}	.0435	.0011
.200			---	---	.072	---	.0430	
.175			---	---	.084	---	---	
.150			.0296	.0331	.084	7.33×10^{-5}	.0429	
.125			---	---	.097	---	---	
.100			.0348	.0425	.095	1.15×10^{-4}	.0424	
.075			.0372	.0483	.094	1.30×10^{-4}	.0416	
.050			.0362	.0539	.082	1.08×10^{-4}	.0557	
.025			.0445	.0732	.087	1.71×10^{-4}	.1273	

*Approximately the same as test 2A High

TABLE 10

SUMMARY OF DATA
DEPTH OF FLOW = 0.3 FT.

TEST 2A LOW
NO RAINFALL

Depth Above Bed z Ft.	Mean Velocity U_m Ft./Sec.	Reynolds Number R ---	RMS Velocity u' Ft./Sec.	Turbulent Intensity $\frac{u'}{\overline{U}}$	Eulerian Length Scale L_T Sec.	Diffusion Coefficient $u'^2 L_T$ $Ft.^2/Sec.$	Sediment Concentration c %	Sediment Diameter d in.
.250	1.03	30,000	.0138	.0174	.137	2.60×10^{-5}	.0085	.0011
.200			---	---	.121	---	.0086	
.175			---	---	.135	---	---	
.150			.0198	.0274	.120	4.70×10^{-5}	.0086	
.125			---	---	.109	---	---	
.100			.0210	.0310	.139	6.11×10^{-5}	.0084	
.075			.0254	.0410	.139	9.00×10^{-5}	.0087	
.050			.0269	.0468	.111	8.03×10^{-5}	.0088	
.025			.0320	.0625	.101	1.03×10^{-4}	.1889	

TABLE 11

SUMMARY OF DATA
DEPTH OF FLOW = 0.3 FT.

TEST 2B LOW
RAINFALL

Depth Above Bed z Ft.	Mean Velocity U_m Ft./Sec.	Reynolds Number R ---	RMS Velocity u' Ft./Sec.	Turbulent Intensity $\frac{u'}{\bar{U}}$	Eulerian Length Scale L_T Sec.	Diffusion Coefficient $u'^2 L_T$ $Ft.^2/Sec.$	Sediment Concentration c %	Sediment Diameter d in.
.250	*	*	.0262	.0307	.0534	3.67×10^{-5}	.0136	.0011
.200			---	---	.067	---	.0127	
.175			---	---	.078	---	---	
.150			.0198	.0258	.079	3.12×10^{-5}	.0158	
.125			---	---	---		---	
.100			.0246	.0342	.089	5.36×10^{-5}	.0124	
.075			.0255	.0375	.087	5.68×10^{-5}	.0130	
.050			.0285	.0448	.093	7.57×10^{-5}	.0123	
.025			.0363	.0665	.095	1.26×10^{-4}	.0544	

*Approximately the same as test 2A Low

GLOSSARY OF SYMBOLS

Symbol		Dimensions
$\underline{A}(t)$	rapidly fluctuating accelerative force vector on a fluid particle	LT^{-2}
A'	constant in the equation for the diffusion coefficient as a function of depth	L^{-1}
$\underline{B}(\Delta\tau)$	average accelerative forces on a particle in the time interval $\Delta\tau$	LT^{-2}
B'	constant in the equation for the diffusion coefficient as a function of depth	L^2T^{-1}
$\underline{D}$	$\int_0^\infty m(t)\,dt$	L^2T^{-3}
D_f	total depth of flow	L
$\underline{G}$	dummy vector	
$H(z)$	notation for the diffusion coefficient as a function of depth	
$\underline{K}$	fall velocity of the sediment particle	LT^{-1}
L_T	Eulerian time scale of turbulence	
$P\left[\underline{x}(t)\right]$	probability of finding a fluid particle at position $\underline{x}$ at time t	
Q_f	volume discharge rate	L^3T^{-1}
Q	probability distribution of displacement of $\underline{X}$ in time t	
R	Reynolds number $= \frac{U_m D_f \rho_o}{\mu}$	
$\underline{R}$	dummy vector	
$R_{ij}(\tau)$	i-j component of the Eulerian correlation tensor	
S	channel slope	
$\overline{U}$	temporal mean velocity	LT^{-1}

Symbol		Dimensions
U_m	mean velocity in the channel	LT^{-1}
V	constant temperature anemometer D.C. voltage	
$c[\underline{x}(t)]$	concentration of sediment at a point $\underline{x}$ at time t	
d	mean diameter of sediment particle	L
e_o	constant temperature anemometer RMS voltage	
g	acceleration of gravity	LT^{-2}
i	$\sqrt{-1}$	
$\underline{m}(\tau)$	covariance kernel of $\underline{A}(t)$	L^2T^{-4}
t	time	T
t_*	time for which the correlation coefficient becomes zero	T
$\underline{u}$	turbulent fluid velocity vector	LT^{-1}
$\underline{u}'$	root-mean-square (RMS) fluid velocity	LT^{-1}
$\underline{u}'^2$	mean square fluid velocity	L^2T^{-2}
$\underline{u}_o$	initial fluid velocity	LT^{-1}
$\underline{v}$	particle velocity vector	LT^{-1}
$\underline{v}_o$	initial particle velocity	LT^{-1}
$\underline{v}'$	root-mean-square (RMS) particle velocity	LT^{-1}
$\underline{x}(t)$	position vector	L
$\underline{X}(t)$	displacement in time t	L
$\overline{\underline{X}^2(t)}$	mean square particle displacement	L^2
z	vertical cartesian coordinate	L
α'	coefficient of King's law	

Symbol		Dimensions
β	particle drag coefficient	T^{-1}
β'	coefficient of King's law	
$\underline{\xi}$	wave number vector	
η	time coordinate	T
μ	viscosity	$FL^{-2}T$
μ_{ij}	i-j component of diffusion tensor	L^2T^{-1}
ε	time coordinate	T
ρ_o	fluid mass density	$FL^{-4}T^2$
ρ	particle mass density	$FL^{-4}T^2$
τ	time coordinate	T
$\Phi(\underline{\xi})$	characteristic function for $P[\underline{x}(t)]$	
$\Psi(\xi)$	dimensionless function of the drag coefficient	
$\Phi_f(\omega)$	spectral density function for fluid velocities	
$\Phi_p(\omega)$	spectral density function for particle velocities	
ω	circular frequency	T^{-1}

LITERATURE CITED

1. Batchelor, G. K. Diffusion in a field of homogeneous turbulence. 1. Eulerian Analysis. Australian Journal of Scientific Research, Vol. 2, No. 4, 1949, 437-450.

2. Batchelor, G. K. Diffusion in free turbulent shear flow. Journal of Fluid Mechanics, Vol. 3, Part 1, Oct. 1967, 67-80.

3. Chadam, J. On a theory of turbulent diffusion. Defense Documentation Center for Scientific and Technical Information Report No. AD-299113, Alexandria, Virginia, 1962, 22 pp.

4. Chandrasekhar, S. Stochastic problems in physics and astronomy. Reviews of Modern Physics, Vol. 15, No. 1, 1943, 1-89.

5. Csanady, G. T. Turbulent diffusion of heavy particles in the atmosphere. Journal of the Atmospheric Sciences, Vol. 20, 1963, 201-208.

6. Gessel, Clyde G. Sediment storage and measurement in the Upper Colorado River Basin. Proceedings of the Federal Inter-Agency Sedimentary Conference, USDA Miscellaneous Publication No. 970, 1963, 778-784.

7. Glass, L. J. and Smerdon, E. T. Effect of rainfall on the velocity profile in shallow-channel flow. Transactions of the American Society of Agricultural Engineers, Vol. 10, No. 3, 1967, 330-332.

8. Hiler, E. A., Curry, R. B., Brazee, R. D., and Schwab, G. O. Colloid movement in a flowing medium with an impressed electric field. ASAE Paper No. 66-738 presented at the Chicago winter meeting Dec. 1966, Accepted for publication Transactions of the American Society of Agricultural Engineers, 39 pp.

9. Hinze, J. O. Turbulence, McGraw-Hill, New York, 1959, Chapter 2, 73-141.

10. Kampe de Feriet, J. Sur un problems d algebre abstraite pose par le definition de la moyenne dans la theorie de la turbulence. Annales de la Soc. Sci. de Burxelles, Ser. 1, Vol. 59, 1949, 145.

11. Leliavsky, Serge. An Introduction to Fluvial Hydraulics, Constable and Co., London, 1959, 257 pp.

12. Laufer, J. Investigation of turbulent flow in a two-dimensional channel. National Advisory Committee for Aeronautics, Report 1053, 67 pp.

13. Meyer, L. D. An investigation of methods for simulating rainfall on standard runoff plots and a study of the drop size, velocity, and kinetic energy of selected spray nozzles. Special Report No. 81, USDA-ARS, May 1958, 41 pp.

14. O'Brien, M. P. Review of the theory of turbulent flow and its relation to sediment transportation. Transactions, Hydrology Section, American Geophysical Union, 1933, 487-491.

15. Raichlen, F. Some turbulence measurements in water. Journal of the Engineering Mechanics, Proceedings American Society of Civil Engineering, Vol. 2, April, 1967, 73-99.

16. Rao, M. V. A study of the shear turbulence in free surface flow. Doctoral Dissertation, Utah State University, Logan, Utah, Sept. 1965, 182 pp.

17. Rouse, Hunter Modern conceptions of the mechanics of fluid turbulence. Transactions of American Society of Civil Engineers, Vol. 102, 1946, 536.

18. Smerdon, E. T. Effect of rainfall on critical tractive force in channels with shallow flow. Transactions of the American Society of Agricultural Engineers, Vol. 7, No. 3, 1964, 287-290.

19. Taylor, G. I. Diffusion by continuous movements. Proceedings, London Mathematical Society, Vol. 20, Jan. 1920, 196-212.

20. Townsend, A. A. The measurement of double and triple correlation derivatives in isotropic turbulence. Proceedings of the Cambridge Philosophical Society, Vol. 43, 1947, 560-571.

21. Vanoni, Vito A. Transportation of suspended sediment by water. Transactions of American Society of Civil Engineers, Vol. 111, 1946, 67-133.